University of São Paulo
"Luiz de Queiroz" College of Agriculture

Proximal and remote sensing on the soil processes: from punctual to spatial approaches

Arnaldo Barros e Souza

Thesis presented to obtain the degree of Doctor in Science. Area: Soil and Plant Nutrition

Piracicaba
2020

Arnaldo Barros e Souza
Agronomist

Proximal and remote sensing on the soil processes: from punctual to spatial approaches

Advisor:
Prof. Dr. **JOSÉ ALEXANDRE MELO DEMATTÊ**

Thesis presented to obtain the degree of Doctor in Science. Area: Soil and Plant Nutrition

Piracicaba
2020

Dados Internacionais de Catalogação na Publicação
DIVISÃO DE BIBLIOTECA – DIBD/ESALQ/USP

Souza, Arnaldo Barros e

Proximal and remote sensing on the soil processes: from punctual to spatial approaches / Arnaldo Barros e Souza. - - Piracicaba, 2020.

81 p.

Tese (Doutorado) - - USP / Escola Superior de Agricultura “Luiz de Queiroz”.

1. Índice de heterogeneidade 2. Homogeneidade de mapas 3. Processos de formação 4. Horizontação 5. Agrupamento I. Título

DEDICATÓRIA

Aos meus pais,

ANDRÉ E ROSIVALDA,

Às minhas avós,

IOLANDA E ANTÔNIA (In memmorian),

À minha esposa,

CAROLINE, que

ME APOIARAM INCONDICIONALMENTE,

DEDICO!

AGRADECIMENTOS

À minha família que me ensinou a ser quem sou e sempre acreditou em mim,

À minha esposa que me acompanhou nas horas mais difícies e nas mais felizes (inclusive nas coletas de dados), cobrou, apoiou, vibrou, brigou (e muito), virou noites comigo no laboratório, e ainda arrumou tempo para me levar à viver experiências além da formação profissional,

Aos amigos que sempre me direcionaram palvras de incentivo, alegria e admiração,

Ao meu Orientador pela incrível paciência e sabedoria em conduzir mentes tão diversas,

Ao grupo de pesquisa mais incrível que eu poderia participar, o GeoCiS, pelo conhecimento compartilhado e risadas,

Aos pesquisadores/instituições parceiras que concederam equipamentos para a coleta de dados,

À população brasileira e às agências de fomento CAPES, CNPq e FAPESP pelos recursos investidos na minha formação,

À ESALQ/USP pelo brilhante trabalho que tem possibilitado,

Ao departamento de Ciência do Solo na pessoa dos professores e funcionários por manterem um ambiente sempre amigável e de excelência,

À cidade de Piracicaba que acolheu minha família e me viu crescer profissionalmente e como pessoa,

Minha ETERNA GRATIDÃO!

CONTENTS

RESUMO

Sensoriamento proximal e remoto em processos de solo: da abordagem pontual à espacial

A caracterização dos solos tem ganhado destaque diante da necessidade de conservação dos recursos naturais afim de promover maior segurança alimentar e ambiental. A grande influência dos solos sobre os recursos hídricos e climáticos há muito foi reconhecida pela comunidade científica. Porém, o conhecimento acerca dos processos predominantes e da variação dos atributos do solo em profundidade e ao longo da paisagem tem sido limitado pelo alto custo das análises químicas úmidas, utilizadas tradicionalmente. Estas análises foram calibradas para utilização rotineira e principalmente para fins agronômicos, deixando a desejar em planejamentos mais abrangentes do uso da terra. Como alternativa à esta lacuna, o uso de equipamentos geofísicos associado a dados de relevo e de satélite tem se mostrado muito útil na caracterização dos solos, tanto da superfície quanto da subsuperfície. Técnicas como a espectroscopia do visível e infravermelho, a fluorescência de raios-X, a susceptibilidade magnética e a condutividade elétrica aparente estão entre as mais utilizadas. Estas tecnologias fornecem informações relacionadas à mineralogia, à dinâmica da água e de solutos, à distribuição granulométrica, à distribuição de elementos no perfil de solo e ao teor de material orgânico, de forma rápida e a baixo custo operacional. Com base nestes dados é possível se fazer inferências acerca das formações geológicas sobre as quais o solo se desenvolveu, dos ciclos de deposição e remoção de partículas bem como da translocação dentro do perfil, o que pode também estar associado a climas pretéritos. Além disso, é possível se identificar a dinâmica dos elementos no perfil do solo, a qual é condicionada pela dinâmica da água no perfil de solo e na paisagem como um todo. Porém, o uso desses equipamentos tem sido frequentemente aplicado apenas na construção de modelos para estimar atributos do solo determinados pelas análises tradicionais. Estas análises contêm erros considerados aceitáveis para aplicação direta, mas que são maximizados e propagados pela modelagem. Neste sentido, a principal proposta deste trabalho é dar base para a caracterização dos corpos de solo, do perfil à paisagem, utilizando-se apenas as informações obtidas com sensores proximais e remotos. Assim, foram propostos índices e formas de observação afim de possibilitar a extração de informações diretamente dos dados obtidos com os sensores. O capítulo 1 trata do estudo da horizontação do solo com sensores espectrais e a fluorescência de raios-x utilizados em trincheiras. O capítulo 2 traz a abordagem com perfis simulados por tradagens até um metro de profundidade com a sugestão do Índice de Heterogeneidade do Perfil baseado em sensores e sua relação com a paisagem. No terceiro é abordada a influência do uso de reflectância de satélite comparado com dados de sensores de laboratório, com e sem preparo da amostra, bem como a qualidade dos modelos gerados para estimar índices de intemperismo. No quarto e último capítulo, estudou-se a integração dos dados de sensores com dados de satélite e de relevo para identificação de ambientes de solo. Neste capítulo é proposto um índice para mensurar a homogeneidade das unidades de mapeamento geradas (ambientes de solo) dado um mapa de referência.

Palavras-chave: Índice de heterogeneidade, Homogeneidade de mapas, Processos de formação, Horizontação, Agrupamento

ABSTRACT

Proximal and remote sensing on the soil processes: from punctual to spatial approaches

The characterization of soils has been highlighted due to the need to conserve natural resources in order to promote greater food and environmental security. The great influence of soils on water and climate resources has long been recognized by the scientific community. However, knowledge about the predominant processes and the variation of soil attributes in depth and throughout the landscape has been limited by the high cost of wet chemical analyzes, traditionally used. These analyzes were calibrated for routine use and mainly for agronomic purposes, leaving much to be desired in more comprehensive land use planning. As an alternative to this gap, the use of geophysical equipment associated with relief and satellite data has been shown to be very useful in characterizing soils, both on the surface and the subsurface. Techniques such as visible and infrared spectroscopy, X-ray fluorescence, magnetic susceptibility and apparent electrical conductivity are among the most used. These technologies provide information related to mineralogy, water and solute dynamics, granulometric distribution, the distribution of elements in the soil profile and the content of organic material, quickly and at low operating cost. Based on these data it is possible to make inferences about the geological formations on which the soil developed, the cycles of deposition and removal of particles as well as the translocation within the profile, which may also be associated with past climates. In addition, it is possible to identify the dynamics of the elements in the soil profile, which is conditioned by the water dynamics in the soil profile and in the landscape as a whole. However, the use of these equipment has often been applied only in the construction of models to estimate soil attributes determined by traditional analyzes. These analyzes contain errors considered acceptable for direct application, but which are maximized and propagated by the modeling. In this sense, the main proposal of this work is to provide a basis for the characterization of soil bodies, from the profile to the landscape, using only the information obtained with proximal and remote sensors. Thus, indices and forms of observation have been proposed in order to enable the extraction of information directly from the data obtained with the sensors. Chapter 1 deals with the study of soil horizonation with spectral sensors and the X-ray fluorescence used in trenches. Chapter 2 presents the approach with profiles simulated where it is suggested a Profile Heterogeneity Index based on sensors and their relationship with the landscape. The third one addresses the influence of the use of satellite reflectance compared with data from laboratory sensors, with and without sample preparation, as well as the quality of the models generated to estimate weathering indexes. In the fourth and last chapter, the integration of sensor data with satellite and relief data for the identification of soil environments was studied. In this chapter, an index is proposed to measure the homogeneity of the generated mapping units (soil environments) given a reference map.

Keywords: Heterogeneity index, Maps homogeneity, Formation processes, Horizonation, Clustering

1. SOIL FORMATION PROCESSES AND HORIZONATION: FROM PUNCTUAL TO SPATIAL SENSING

ABSTRACT

Soil layers and horizons have been described in the field by Pedologists who have enough knowledge about a given region. Although limited alternatives have been used to describe the soil by equipments under natural conditions. Therefore, we must expend efforts on applying the newest technologies on these studies. We have proposed to use Vis-NIR and X-Ray Fluorescence (portable) equipments to predict soil horizonation and its process. The main objectives were: i) Identify mineralogical differences between horizons, with inferences about translocations and geochemical alteration by proximal sensors; and ii) Expand the punctual information with RGB images and Digital Surface Model obtained by unmanned aerial vehicle. Seven soil profiles (Acrisol, Cambisol and five Ferralsols) were analyzed in a São Paulo, Brazil region. The data were vertically collected in the field with a Vis-NIR-SWIR (350 – 2,500 nm) spectroradiometer and with a Portable X-ray Fluorescence (pXRF). Dried samples from each layer were analyzed by a Middle Infrared (MIR) (2,500 – 20,000 nm). When with exposed soils, images were taken by UAV and Terrain derivatives were built by stereoscopy. Proximal sensors allowed to perform more robust hypothesis about soil formation processes. On-the-go proximal sensor allows to describe and better understand how soil bodies behave on the landscape. The clusterization with high density data from sensors allows to better describe soil profiles horizonation. The Vis-NIR-SWIR spectral range relationship together with soil color, provides better correspondence with traditional field observation. The combined use of Vis-NIR-SWIR, MIR and pXRF allows to identify the horizon boundaries more appropriately. There was a limit between the surface color of each profile and relief which took an important spatialization by UAV data. From profiles to spatial dimension, relief plus RGB of UAV indicated important delineation of soil units.

Keywords: Pedological distances; Clustering; Vis-NIR-SWIR; MIR; pXRF; Proximal Field Sensing; Digital Soil Mapping.

1.1. INTRODUCTION

Soil and their ecological functions are a result from soil-forming processes (Breemen and Buurman, 2002). Soil genesis drives the properties of soil natural bodies as well as how they interact with biotic and abiotic factors. The horizonation is a registry of these processes and can inform us about ecological functions and resilience capabilities of soils. Hartemink and Minasny (2014) highlight the old premise stated by Jenny (1941) that soil properties variation in depth depend on several factors. Consequently, it is necessary to comprehend how such variation occurs and how could we detect and map the attributes' depth functions. Therefore, we must expend efforts on applying the newest technologies on their studies.

Traditionally, soil layers have been described in the field by pedologists using their senses and based on their tacit knowledge. However, even the soil color information is

different from a pedologist to another (Campos and Demattê, 2004). Nowadays, there are alternatives to describe soil bodies in the field, which provide insights on how they develop and behave on the landscape. However, it is still challenging to describe soil profiles under natural conditions. Spectroscopic techniques, such as portable X-Ray Fluorescence (pXRF), are among the most promising alternatives to solve it (Weindorf et al., 2014; Zhang and Hartermink, 2019a). Once it does not need sample preparation nor chemical products, they allow to obtain high density data directly in the field (Stockman et al., 2016).

Another promising method correspond to field spectroscopy (Viscarra Rossel et al., 2009). The electromagnetic energy in visible, near and shortwave-infrared (Vis-NIR-SWIR: 350 to 2,500 nm) and middle-infrared (MIR: 2,500 to 25,000 nm) regions interacts with matter by low energy emissions (Viscarra-Rossel et al., 2006 and 2009). Such interactions allows the acquisition of information about soil mineralogy and organic carbon content (Stenberg et al., 2010). These soil attributes are the main expression of the soil abiotic and biotic forming processes.

The clay translocation (argiluviation), one of the most evident soil forming process result was modeled by Souza et al. (2020) showing its relationship with spectral data (Vis-NIR-SWIR and MIR). The authors identified wavelengths that were highly correlated to clay content and used it to find the ratio of clay in 150 soil profiles. Additionally, the specific bands occurrence related to mineralogical compounds is well known (Stenberg et al., 2010; Terra et al., 2015). This fact allows to understand the predominant processes related to hydrology, once it drives the mineralogical assembly in the soil profile. Tropical soils are known by having highly altered compounds due to the high precipitation (Buol, 2005).

Nevertheless, the abundance elements through soil profiles are also important to characterize the soil evolution once soil processes can redistribute it on the landscape (Weindorf et al., 2014). The X-Ray Fluorescence is a primary method based on the interaction between X-Rays and atoms and is useful on measuring elemental distribution on soil bodies (Stockmann et al., 2016; Zhang and Hartermink, 2019a). However, spectroscopic sensors have many variables as output which leads to the need for statistical approaches to extract the required information. Clustering analyses are one of the most useful procedure in cases when ones need to identify groups. This analysis enables to identify how the soil horizons can be grouped on the profile based on sensor data. Fajardo et al. (2016) and Zhang and Hartemink (2019a) used pXRF and Vis-NIR-SWIR data to recognize and delineate morphological horizons in soil profiles and found good results.

Despite the punctual (profile) view, the hydrology as well as matter flows on the landscape is determined by the landforms and the concatenation of soil bodies (Breemen and Buurman, 2002). Thus, the spatial vision needs to be considered on the soil formation understanding (McBratney et al., 2003). Landform information can be well represented by terrain derivatives, which can be obtained from RGB images registered by using an Unnamed Aerial Vehicle (UAV) and stereoscopic algorithms. Thus, terrain derivatives, such as Topographic Wetness Index and Relative Slope Position, can be used together with RGB data to characterize the surface dimension and to be linked with soil profiles as a mutually influencing factors.

The main challenge of this approach is to link and understand the relationships between data from soil profile and those from surface, because the landscape was built over thousands of years. In fact, this is the main contribution from the present work. In this context, we proposed to use Visible-Infrared spectroscopy and X-Ray Fluorescence to infer about soil forming processes and horizonation as to link with RGB image and Terrain derivative attributes obtained with an Unnamed Aerial Vehicle. The main objectives were to: i) Identify mineralogical differences between horizons, make inferences about translocations and geochemical alterations by spectroscopy and X-Ray Fluorescence; ii) Evaluate the horizonation by clustering with Visible-Infrared and X-Ray fluorescence data compared to field observation; iii) Expand the punctual vision by aerial RGB images and Terrain derivatives obtained with an unmanned aerial vehicle.

1.2. MATERIAL AND METHODS

1.2.1. Study site

The study site is located in the Itu municipality, São Paulo State, Brazil (Figure 1). The climate is classified as Cfa, according to Köppen and Geiger (Alvares et al., 2013). The average temperature is 19.5°C and the average annual precipitation is 1,279 mm. Acrisols, Cambisols and Ferralsols are the main soils in the area (Oliveira & Prado, 1983), which are commonly strongly weathered and poor in plant nutrients. Sedimentary and magmatic rocks from the Itararé and Serra Geral formations are the main parent materials (Mezzalira, 1989). The elevation is from 573 to 658 m and the landforms are predominantly convex.

1.2.2. Data collection

Seven soil profiles were excavated to 2 m depth (Figure 1), described and classified according to Brazilian Soil Classification System (Santos et al., 2018) and Word Base Reference for Soil Resources (WRB, 2014). Spectroscopic data were collected in the field with a Vis-NIR-SWIR spectroradiometer and a Portable X-Ray Fluorescence (pXRF) at 0.1 m depth increments (Figure 2). Then, samples from each layer were collected to allow measurements with a Mid-infrared (MIR) equipment in the laboratory.

The Vis-NIR-SWIR spectra were registered by a FieldSpec 3 spectroradiometer (Analytical Spectral Devices, ASD, Boulder, CO), which has a spectral range from 350 to 2,500 nm. It was taken The spectral resolution varies for each spectral range, as follows: 1 nm, from 350 to 700 nm; 3 nm, from 700 to 1,400 nm; and 10 nm from 1,400 to 2,500 nm. However, the output data were resampled to 1 nm, resulting in 2,151 channels (Demattê et al., 2019). A contact probe connected to an optic fiber cable and to a light source was used to allows the data collection without changes on the photon flux. A white spectral plate was used as a maximum reflectance reference (Figure 2).

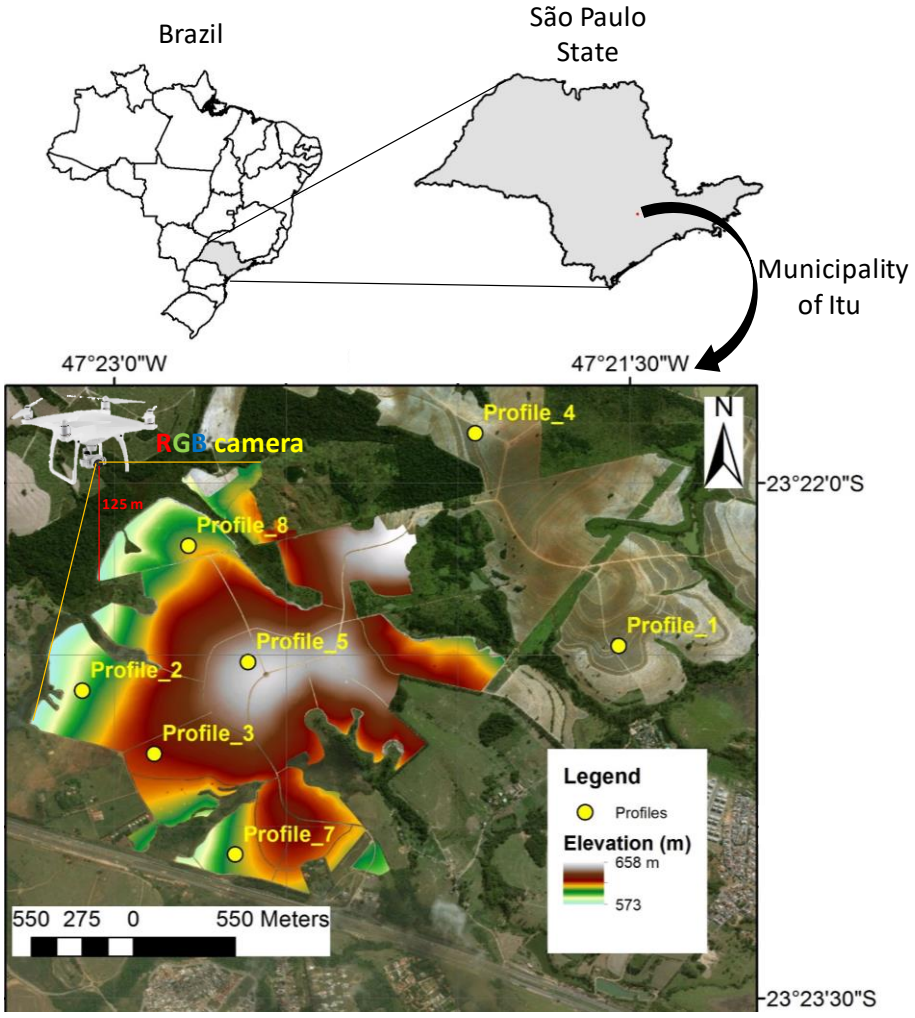

Figure 1. Localization of the study area, elevation model obtained with an unnamed aerial vehicle (UAV) and soil profiles location). Profile 4 and 1 does not have UAV information.

The pXRF equipment works with a Silver anode (Ag) X-Ray tube (4 W) in the range from 0 to 40 keV. Calibration was checked by using the NIST 316 alloy, two standard soil samples (SRM 2710a – Montana I Soil; and SRM 2711a – Montana II Soil) and a pure SiO2 sample, both from NIST. It was used two energy beans to optimize the light elements estimation: 0 to 10 keV and 0 to 40 keV. This procedure (0 to 10 keV) improves the signal/noise ratio allowing to get better estimations once high energy scattering increases the noise at low energy channels. The equipment was used on “Soil” mode, which is an internal software that allows to estimate the elements concentration in soil-like matrices. The pXRF interacts with matter in an atomic level reporting the chemical composition of the sample for

elements with atomic number above 11. This is a primary method based on direct interactions between X-ray energy and elements so it can provide relative elemental concentration of the samples (Weindorf et al., 2012a).

The soil samples were dried at 45 ºC, sieved to 100 mesh, disposed in a bucket, smoothed with a spatula and submitted to a Diffuse Reflectance Infra-Red Fourier Transformed (DRIFT) in the Middle Infrared (MIR) range (2,500 to 20,000 nm) (Figure 2). The data from each sample were obtained with 32 readings with 2 cm-1 channel width resampled to 1 cm-1, totalizing 3,432 channels. Each wavenumber (cm-1) were transformed to wavelength (nm) dividing by 10.000.000. A gold plate was used as reference for the maximum reflectance for every profile.

1.2.3. Data processing

The pXRF data were used to calculate the following indices: (Si/Al (Ruxton, 1968); Fe/Al; Si/(Al+Fe) (Ruxton, 1968); Si/Fe; Chemical Index of Alteration (CIA) (Nesbitt and Young, 1989); Chemical Index of Weathering (CIW) (Harnois, 1988); Plagioclase Index of Alteration (PIA) (Fedo et al., 1995); Ti/Zr (Maynard, 1992); Zr/Sr and Rb/Sr (Dasch, 1969); Ca/Ti (Betard, 2012); and SiTi index (Jayawanderna and Izawa, 1994). It was assumed that the Si and Ca are mobile and the others are immobile during the weathering process. The Si/Al ratio (Ruxton, 1986) informs the loss of silica due to soil evolution process. The Ti/Zr ratio allows to infer about parent material differences because these elements are highly correlated and little affected by primary minerals alteration (Maynard, 1992). The Ca/Ti ratio was proposed by Betard (2012) as a complementary mobile/immobile index. The Si/Ti index is a ratio between Si and Ti and Al (Jayawanderna and Izawa, 1994). The Chemical Index of Weathering (CIW) (Harnois, 1988) considers the ratio between Al oxide and Ca and Na ones and ranges from 0 to 1.

Both of the sensors used in the field are affected by soil moist, which reduces the soil reflectance on Vis-NIR-SWIR region and increases the scattering on X-Ray Fluorescence. However, the data from these sensors were not processed to avoid these effects aiming to show the potential of raw data on soil horizonation studies in field conditions. Besides that, Stockamn et al. (2016) showed that XRF data acquired in field conditions are comparable to that acquired in air-dried samples.

The data obtained in the field (VIS-NIR-SWIR and pXRF) and laboratory (MIR) were submitted to a k-means clustering analysis to access the similarities among layers from a same soil profile. The clustering analysis was performed in R by using the "Cluster" (Maechler et al., 2019), "ClusterCrit" (Desgraupes, 2018) and "plyr" (Wickham, 2011) packages. The ideal number of clusters for each soil and each data set was accessed by the Calinski-Harabasz pseudo F-statistic approach (Calinski and Harabasz, 1974). Four clustering datasets for each soil profile were performed as follows: Vis-NIR-SWIR, MIR, pXRF indices, and for all data together. This approach was used to show the potential of each one on identifying pedological layers and make easier to understand each cluster. Because of the variable output amount and the high correlation between bands, the Vis-NIR-SWIR and MIR data were reduced by principal component analyses and the first four components were used on the clusters building.

1.2.4. Spatial data collection and processing

An unmanned aerial vehicle (UAV) with a RGB camera were used (Figure 2), in order to obtain remote surface information. The flight was performed at 125 m height with 70% coverage between the images. This configuration allows to obtain a Ground Sample Distance of 0.03 m and to generate a Digital Surface Model (DSM) by stereoscopy using the Agisoft Photoscan software (Agisoft, 2016). The RGB images were separated into single bands, i.e., each band were used separately. Twelve terrain derivatives were calculated from the DSM using the SAGA GIS v. 2.1.4 software (Conrad et al., 2015): Elevation; Valley Depth (VD); Vertical Distance to Channel Network (VDCN); Channel Network Base Level (CNBL); LS-Factor (LSF); Topographic Wetness Index (TWI); Catchment Area (CA); Convergence Index (CI); Longitudinal Curvature (LC); Cross-Section Curvature (CSC); Slope; Analytical Hillshading (AH); and Relative Slope Position (RSP) (Figure 2).

All information derived from UAV data (i. e., Terrain derivatives and RGB) were sampled to punctual view on 370 points (1/ha). This approach was used to reduce the noise due to the ultrahigh spatial resolution (0.03 m) without losing details in such high resolution. The terrain derivatives from points were used to generate new variables by Principal Component Analyses. The first three components were used to characterize the occurrence of profiles in the landscape.

The points were classified by using the Grouping function implemented in the ArcGIS software with K-Nearest Neighbors by using the first three principal components and the RGB data. The area where the profile 8 occurs does not have bare soil RGB data once it was covered by plants during the flight. The points group were used to build a surface by Spline method (Franke, 1982), which generate a smooth surface varying gradually through the points. The three closest points of each profile were selected for graphical demonstration of the relief and color attributes that characterize each one of them.

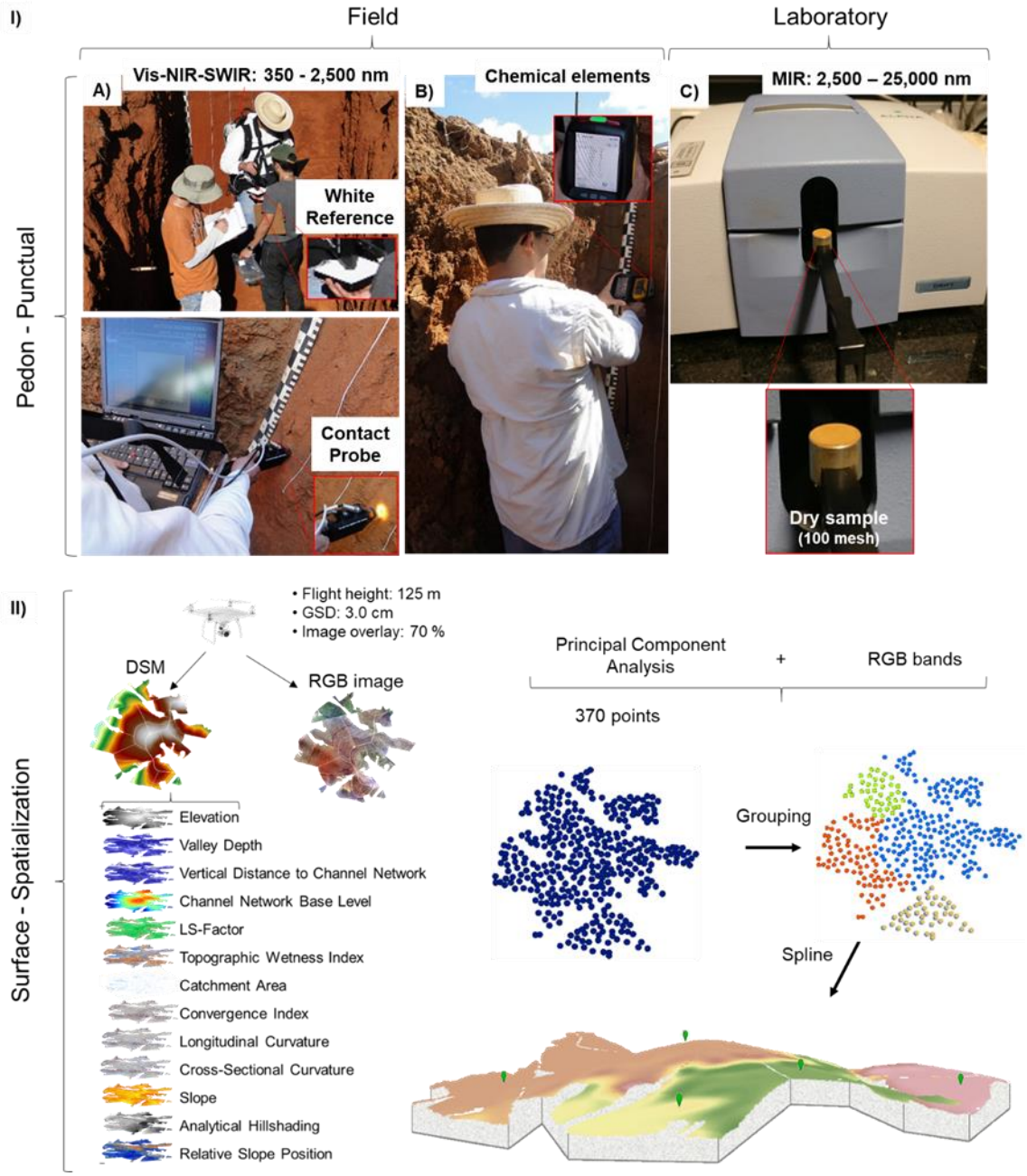

Figure 2. Methodology flowchart. I) Sampling and data collection on soil profiles: A) Vis-NIR-SWIR; B) Portable X-Ray Fluorescence; C) Middle Infrared (MIR). II) Spatial data collection, derivative attributes and mapping.

1.3. RESULTS AND DISCUSSION

The data from sensors showed high correspondence with horizons as described by traditional field observation (Figures 3-6). The differences between layers are evidenced and

allows to better identify the horizons boundaries. The mineralogy assembly was comprised of kaolinite, gibbsite, quartz and iron oxides (Figures 3-6), as expected for tropical soils (Buol, 2005). The CIA, CIW and PIA indices were constant through in depth of all profiles, denoting the high weathering in all studied soils.

The Xanthic Acrisol horizons (Profile 1, Figure 3A) were very well delineated by cluster analyses. This soil type have horizons very different from each other due to the vertically translocation of clay (argiluviation), forming argic horizons (Lessivage: WRB, 2014). A horizon differs from E horizon mainly because of the organic matter content, whereas E horizon from Bt3 horizon due to the clay content, that was maximal in the B horizon (Figure 3A).

All of those differences affect the energy reflected in the Vis-NIR-SWIR and MIR range by the core sample and the elements abundance detected by pXRF on the soil profile. All data clustering (Vis-NIR-SWIR, MIR and pXRF indices) suggested a more detailed horizonation between A and E horizons and from E to B ones than that from tacit observations. This was expected once the approach involves multiple levels of observation, i. e., from molecule to atomic level. However, this approach did not differentiate B horizons between themselves, which could be related to the main challenge in the proximal sensing: the soil structure. Ultimately, the Xanthic Acrisol horizons (Figure 3A) could be differentiated by sensors data clustering, where MIR and XRF showed more detailed information, as expected due to the fundamental bands (MIR) and to the elemental level of interaction (pXRF). However, the differences inside of the A-E layer where more evident in pXRF profiles (Figure 3A), which supports the fact of a stronger dynamic of the elements than that of the molecules. This fact is particularly interesting for Ca/Ti ratio (Figure 3A), which shows a maximum and minimum profile from Ap to the B horizon top. This behavior could be related to hydrodynamics and may be helpful on the understanding of the processes on this profile.

The cluster analysis performed for profile 1 with the Vis-NIR-SWIR spectral region was not able to separate E from Bt horizon (Figure 3A). These results were not expected due to the high matrix contrast and disagree from those obtained by Terra et al. (2018). The authors report that the spectral differences between albic and argic horizon is very expressive due to the contrast of spectrally active attributes between them. In the present case, this fact may be due to the field moist, as observed by Zhang and Hartemink (2019a), who did not distinguish E horizon with a cluster method with moist data by using proximal sensors. However, the authors observed that the measurement with a Vis-NIR-SWIR sensor on moist soil samples performed better than those measured on dry soil samples for the purpose of soil

horizon delineation. This fact could be related to color observation in the field, because the moist on the soil profile affects the color perception from the pedologists. In fact, human eyes are more sensible when soils are moist because the water covers the particles and makes the energy to be more absorbed (Campos & Demattê, 2004). On the other hand, moist can mask other elements on sensors range and take out the linearity between spectra and soil properties (Viscarra-Rossel et al., 2016).

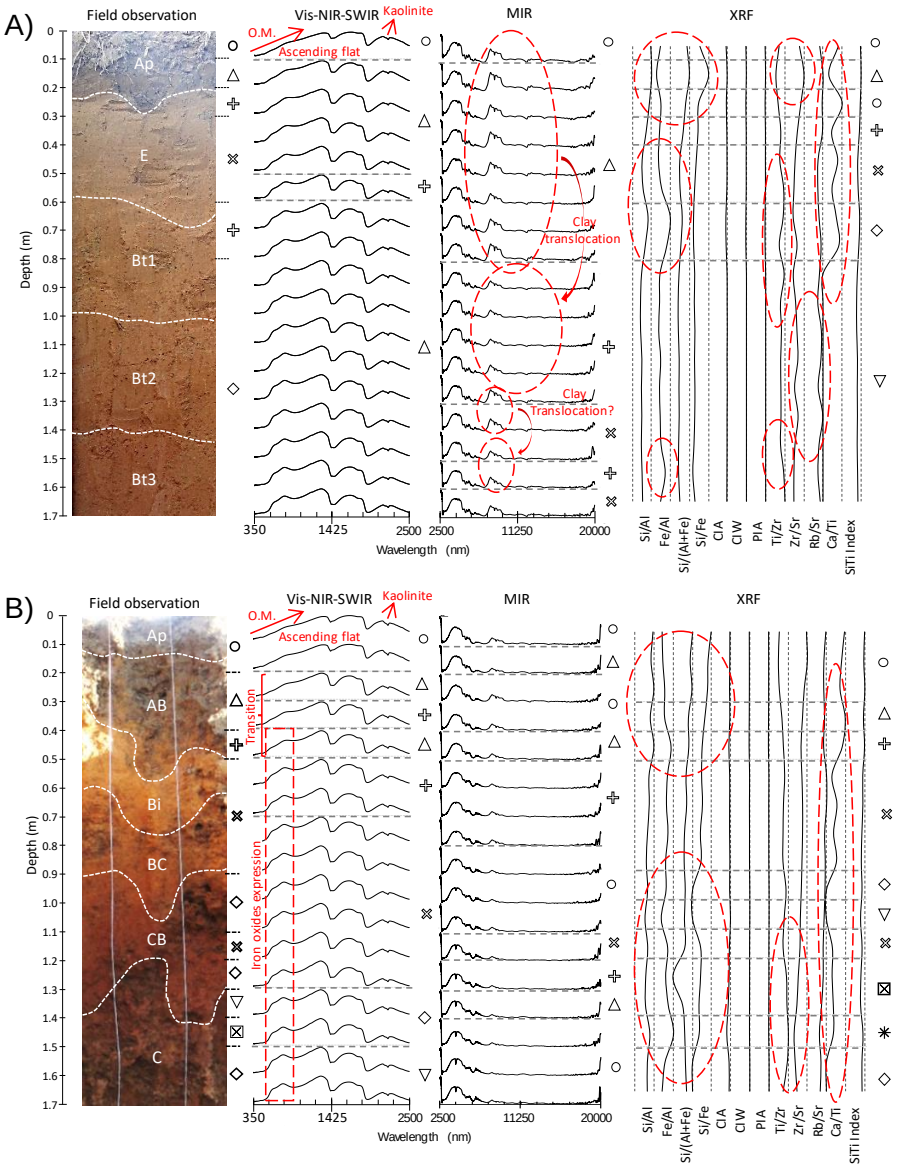

Figure 3. Soil profiles horizonation by tacit knowledge and by clustering from spectral and pXRF data (0.1 m spatial resolution). A) Profile 1: Xanthic Acrisol (Argissolo Vermelho-Amarelo distrófico - SiBCS); B) Profile 2: Clayic Dystric Cambisol (Cambissolo Háplico Tb distrófico - SiBCS).

The clustering with MIR data delineated the three main horizons, i. e., A, E and B (Figure 3A). However, it suggested a new bounding between E and B horizons, which would

be around 0.80 m. The contrast concerning these two horizons is very strong and can be easily seem in the MIR signatures on the main clay absorption bands (from 7,692 to 9,520 nm), which is due to the O-Al-OH deformation and to the Si-O-Si elongation (Terra et al., 2015). Also, the quartz specific expression in the MIR spectra, which do not occur on Vis-NIR-SWIR region, associated to dried sample, could contributed to this results. On the other hand, the differences between B horizons were not well defined based on the MIR range. The curve analysis suggested more than one cycles of clay translocation, that is, from 0-0.80 to 0.80-1.20 m and from 1.20-1.40 m to 1.40-1.60 m. This fact could suggest a material superposition during the soil development history, which is not well explored in the literature because of the limitation on soil sampling and analyses regarding soil classification, when it is taken few samples from the B horizon. These facts are supported by XRF analyses.

The differences between A and E horizons (Figure 3A) were expressed by the following indices from pXRF: Si/Al; Fe/Al; Si/(Al+Fe); Si/Fe; Zr/Sr; Rb/Sr and Ca/Ti. These facts were due to the Fe and Al translocation from A and E to B horizon on this soil profile. Zhang and Hartemink (2019a) studied soil horizonation by vis-NIR and pXRF and observed a decreasing Ti/Zr and Ca/Zr ratios in A horizon, which was constant in E and B horizons. Those authors found even a constant Fe/Zr ratio for A horizon, which was crescent in the E and Bt horizons.

The Si/Al and Fe/Al ratios showed a peak function around the E-B boundary (Figure 3A). This fact could be associated to the ferrolysis process, which consists on the clay destruction due to the H+ released by Fe redox reaction cycles (Brinkman, 1970; MCDaniel et al., 2001). These cycles occur on the top of the B horizon due to the lower hydraulic permeability in this layer, causing alternate oxidation and reduction events (van Ranst and Coninck, 2002). The Ca/Ti ratio showed a very strong boundary on E-B transition, which should be associated to the Ca addition (due to agriculture management) and translocation on the soil profile. Weaker bounds that corroborate this fact can be seen on the Zr/Sr and Rb/Sr ratios. It is expected once Ca and Sr have similar behavior on the soil profile being solubilized during the soil weathering process (Bokhorst et al., 2009). This agrees with Weindorf et al. (2012) which used pXRF to improve the differentiation of Spodic and Albic horizons. The authors related the usefulness of the elemental ratios for differentiating volcanic ash from true E horizons. The boundaries showed in Fe/Al, Ti/Zr, Zr/Sr and Rb/Sr ratios between 1.30 and 1.60 m depth corroborates the hypothesis of clay translocation raised in the MIR discussion. In fact, the behavior of these indices are very similar in both of the transitions. Bokhorst et al.

(2009) pointed out that Rb and Zr are considered immobile in the soil profile and highly adsorbed on clay minerals.

The profile 2 (Clayic Dystric Cambisol, Figure 3B) all data clusterization suggested many transitional clusters, as expected for this soil type. Cambisols are characterized by weak pedological development due to restrictions imposed by soil formation factors, mainly parental material and relief (Schaetzel, 2005). In the present case, the limitation is the relief, once the parent material has enough clay to structure development and horizon differentiation, which can be confirmed on the spectral signatures.

The clusters from Vis-NIR-SWIR for profile 2 (Figure 3B) best matched the field-based horizon identification. It was expected once both of the approaches has the Visible region as the main data source for horizon delineation. However, the MIR data does not allow to identify a logical horizon sequence. Ap horizon was classified in the same group as C horizon with the MIR data. This fact could be associated to their weak pedological development and to the irregular transitions between horizons. Thus, in this case, Vis-NIR-SWIR range worked better than the MIR one.

The indices from pXRF showed a high dynamic processes of the elements for the Cambisol (Figure 3B). The Zr/Sr and the Rb/Sr ratios decreases with depth once Ti/Zr increases. The XRF data showed an A-B more expressive boundary by the Si/Al, Fe/Al and Ca/Ti ratios (Figure 3B). Zhang et al. (2019a) found large differences for the Ca/Zr ratio among horizons; The B-C differentiation on the profile 2 was showed mainly by two minimum points. The Si/Fe and the Ca/Ti ratio suggested a Si and a Ca depletion, respectively. Silva et al. (2018) studied an Inceptisol from the Brazilian Cerrado and observed a considerable elemental variation either with the depth and between horizons. The authors reported greater contents of Ca, K, Al, Rb and other in the Cr horizon and do not found out a pattern for Ti, Fe and Cu.

The Ferralsols showed the most homogeneous spectral layers signatures and elemental abundance profiles (Figures 4-6). This soil type is characterized by being strongly weathered and homogenized by proisotropic pedoturbation (Johnson et al., 1987). The Ferralic weathering (or Ferralitization) is a characteristic process that lead to the Ferralsols formation, which is characterized by the bases and silica losses and iron and aluminum accumulation (Breemen and Buurman et al., 2002). The sensors allowed to identify horizons with very similar boundaries to those described on the field by tacit observation (Figures 4, 5 and 6). The Si/Fe and Ca/Ti ratios were the most expressive ones on the A-B differentiation to the profile 3 (Figure 4A).

A horizon of the profile 4 (Figure 4B) was distinguished from B1 horizon mainly by Si/Al, Si/(Al+Fe), Si/Fe and Ca/Ti indices. A depletion peak on Si/Fe and Ca/Ti profiles match the B1-B2 boundary. This fact could be related to the wetting front, which also explains the differences in observed color between both of these horizons. The B1 have more goethite than B2, which can be inferred by the yellowish on the first one (Figure 4B). This oxide is formed on more humid conditions and is also favored by organic matter iron complexation (Schaetzl, 2005). Another Si/Fe depletion peak can be seeming from 0.80 to 0.90 depth layer, which supports the idea of a subdivision of this horizon (may be a BC horizon). This fact is supported by the changes on the Zr/Sr, Rb/Sr and Ca/Ti ratios.

The flattest transitions between horizons can be seen on the profile 5 (Figure 5A). The clusters obtained with Vis-NIR-SWIR was very similar to that obtained from traditional field observation. This fact is due to the color's assessment in this region, attribute that is one of the most important on pedological horizons distinction by traditional method (i.g. human vision). Grauer-Gray and Hartermink (2018) delineated the soil horizons boundary based on soil organic carbon content, texture and color. The authors concluded that the method improve field delineation of soil horizons. Zhang and Hartemink (2019c) used images color and texture to develop an automated method to identify horizons in ".JPG" format.

In the MIR spectral region (Figure 5A), the clusters distribution allows to infers that some kind of translocation occurs in the B horizon of this profile. These evidences could be seen on the clay absorption bands and were corroborated by pXRF peaks (layer between 1.3 and 1.4 m - Fe/Al; and 0.6 and 0.9 m - Si/Fe). The A-Bw1 transition is strongly expressed by Si/Al, Si/(Al+Fe), Zr/Sr, Rb/Sr, Ca/Ti and SiTi indices (Figure 5A). From Bw1 to Bw2 it is possible to observe a strong absorption due to clay minerals O-Al-OH deformation (around 8,640 nm) in the MIR spectra. This transition is also marked in Si/Fe and Ti/Zr ratio. A similar transition on MIR spectra can be seen from the layer located in the 1.3 to 1.4 m region. The clay expression increases drastically and turns to be stronger every layer. This fact occurs in three sequences in Bw horizons (from layer 5 to layer 8; from layer 9 to layer 14; and from layer 15 onwards). This fact suggests a cyclic change on soil texture which can be an evidence of climate and soil forming phase changes

Although Ferralsols are characterized by having homogeneous profiles, the stable surface associated to climate changes make these kind of soils having a polygenetic formation which could remain registered on the soil profile through the soil evolutionary history (Muggler and Buurman, 2000). These authors highlighted that, even though these evidences could be abundant, to separate the phases (or periods) of soil formation is not easy. This fact

is reinforced by the inherent bioturbation, which greatly affects the physicochemical processes that occur in the soil bodies.

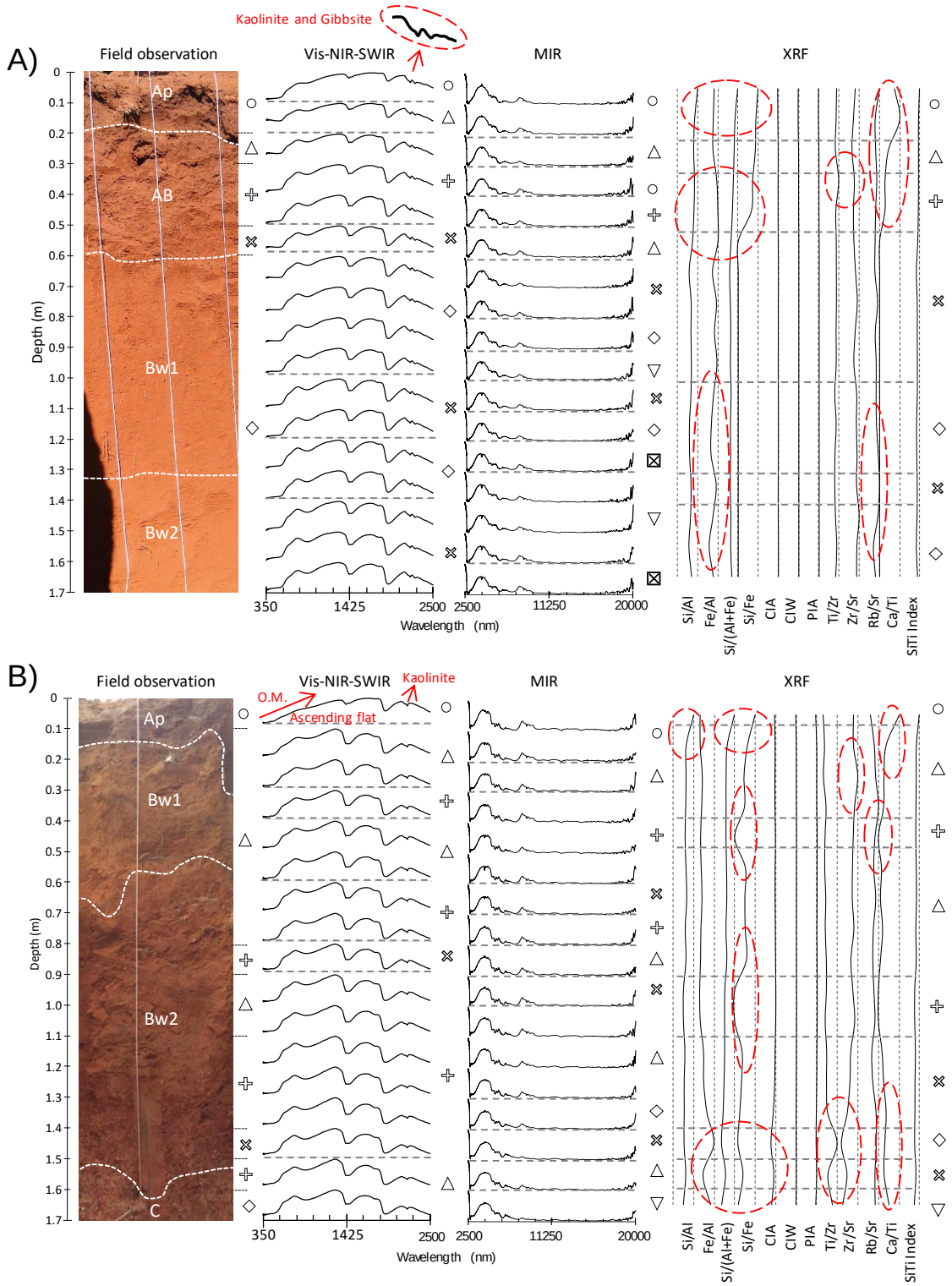

Figure 4. Soil profiles horizonation by tacit knowledge and by clustering from spectral and pXRF data (0.1 m spatial resolution). A) Profile 3: Dystric Xanthic Ferralsol (Latossolo Vermelho-Amarelo distrófico - SiBCS). B) Profile 4: Dystric Xanthic Ferralsol (Latossolo Vermelho-Amarelo distrófico - SiBCS).

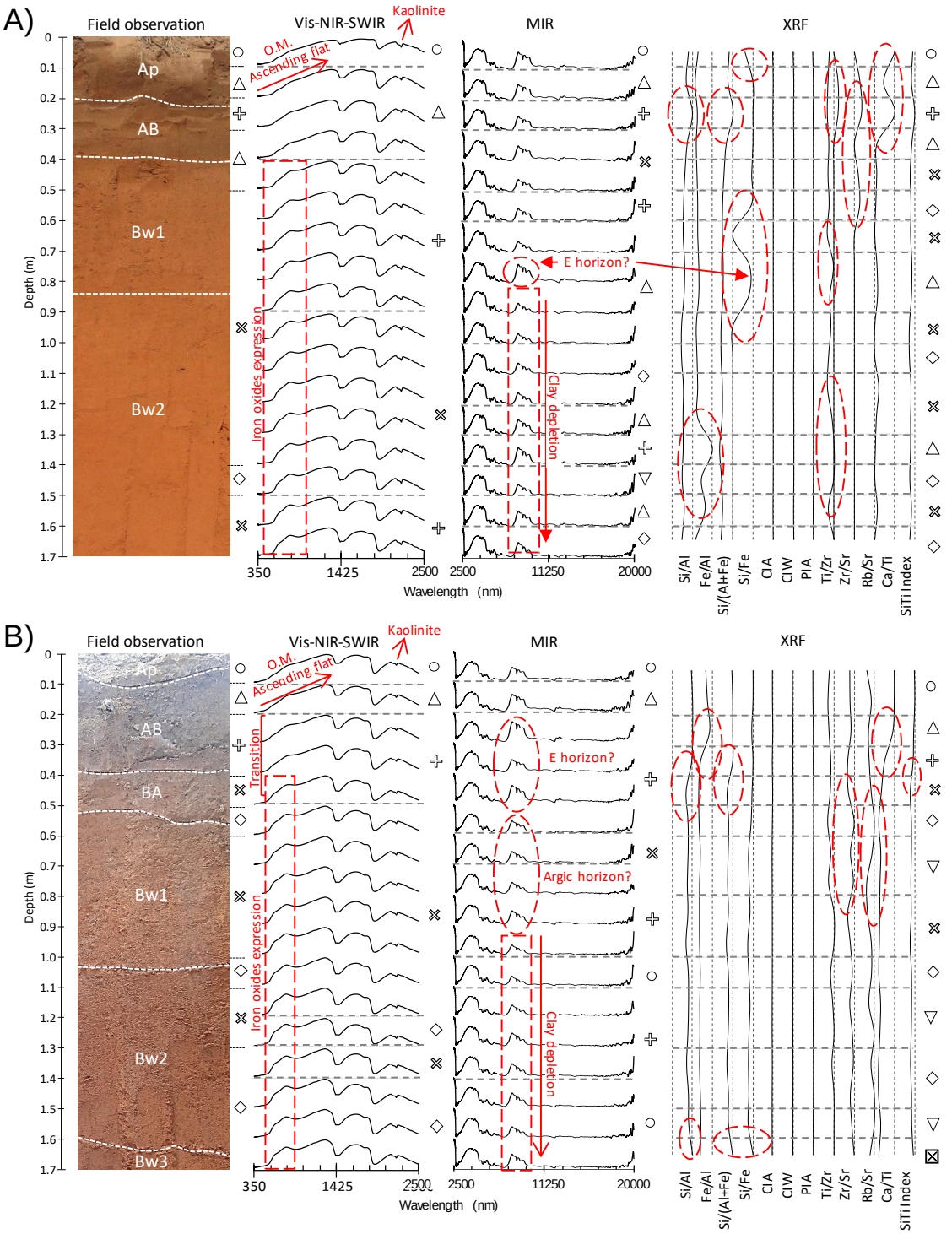

Figure 5. Soil profile horizonation by tacit knowledge and by clustering from spectral and pXRF data (0.1 m spatial resolution). A) Profile 5: Dystric Xanthic Ferralsol (Latossolo Vermelho-Amarelo distrófico - SiBCS). B) Profile 7: Dystric Rhodic Ferralsol (Latossolo Vermelho distrófico - SiBCS).

Terra et al. (2018) using Vis-NIR spectra showed evidences of residual accumulation of Fe, Al, Ti sesquioxides in Ferralsols but without clay migration. The first hypothesis is against the proisotropic pedoturbation process, which is one of the most expressive one on Ferralsols, or it is an evidence that this process occurs in a limited layer on each event. The other one could be explained by clay translocation. This process is not frequently reported occurring in Ferralsols, beause the strong microaggregation that involves Fe and clay do not favor this clay movement. However, pXRF indices profiles supports the idea of material movement on this soil profile (Figure 5A). Terra et al. (2018) used Vis-NIR spectra to study soil classes based on weathering and pedogenesis and stand out the desilication, ferralization and leaching as the main processes that drives the Ferralsols development. However, the bioturbation is an inherent process that also drives the Ferralsols genesis and can lead to layer differentiation during the soil formation (Muggler and Buurman, 2000).

The homogeneity is more expressive on profile 7 (Figure 5B). Nevertheless, the clusterization shows a kind of cyclic similarity between layers when all the four dataset were combined. The indices profile transitions were more like the duplex type with changes in a short space (Si/Al; Fe/Al; Si/(Al+Fe; Ca/Ti). This kind of change is associated to wetting front (Minasny et al., 2016) and could be an evidence of the depth that the rainfall events more commonly hit by gravitational water. Below, the capillary water moves through smaller pores and with high pressure, which reduces the material transportation.

The Vis-NIR-SWIR spectra clusterization from profile 8 (Figure 6) shows the same horizonation as the traditional one, except for Bw1-Bw2 transition. This fact is due again to the colors being very different from each horizon. An improvement of clay absorption bands expression and a minimum-maximum-duplex behavior of the Si/Fe were coincident around layer 1.1 m depth. Changes in the Zr/Sr and Rb/Sr ratios also occurs at the same depth. Minasny et al. (2016) observed a uniform Ti/Zr ratio throughout the soil profile with an increasing value in the Bw3 horizon, which could be due to clay/sand differences. These evidences support the theory of Ferralsols polygenetic formation. In fact, the use of spectroscopic sensors and a pXRF allows to raise hypothesis about soil formation history due to the high spatiotemporal resolution and portability. However, the full understanding of the soil genesis depends on the surface hydrodynamics, which is driven by soil profile organization and landforms.

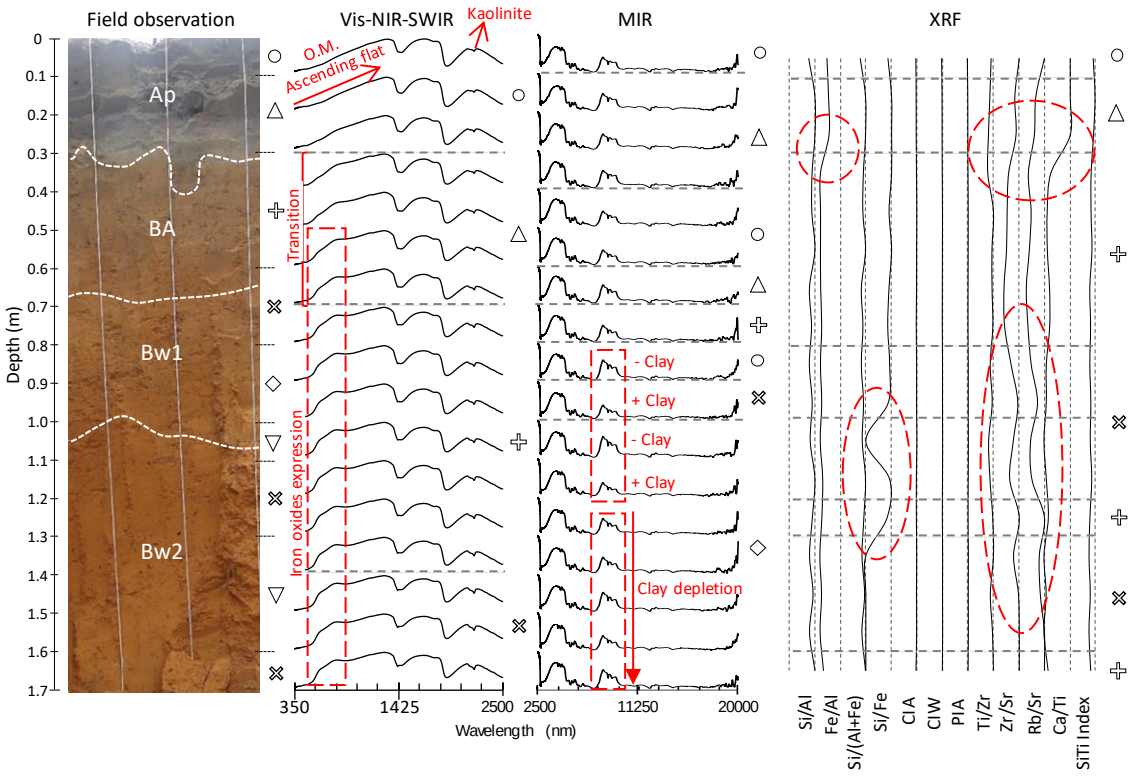

Figure 6. Soil profile horizonation by tacit knowledge and by clustering from spectral and pXRF data (0.1 m spatial resolution). Profile 8: Dystric Xanthic Ferralsol (Latossolo Vermelho-Amarelo distrófico - SiBCS).

The map based on surface data shows a compartmentation highly associated to the soil profiles and is useful on the soil occurrence on the landscape (Figure 7, A-D). It is evident the occurrence of soils with contrasts in the clay content. Profiles 2 and 3 have more clay than the other ones and are concatenated on the landscape, which suggests that they developed on a similar parent material. However, their morphology is completely different from each other. The terrain attributes could explain this fact. The profile 2 (Clayic Dystric Cambisol) occurs in the lowest Relative position (Figure 7B), which could explain the mixing observed among its horizons because of the depositional events. The relative position on the landscape defines the export and depositional processes and can drive the horizonation on the soil profile (Breemen and Buurman, 2002). The gibbsite occurrence on the profile 3, evidenced by its Vis-NIR-SWIR spectra (Figure 4A), could even be associated to the terrain attributes. This profile is in a higher position and in a flattest landform which favors chemical alteration and solution removal (Figure 7). The gibbsite formation is due to the allitization process which is an advanced stage of weathering in which Fe and Al accumulate (Schaetzl and Anderson, 2005). This mineral formation is possible only in a highly intense weathering environment,

which can be conditioned by the landforms and relief context (Figure 7) where this soil profile developed (Dixon, 1989).

Among the sandy profiles (profiles 5, 7 and 8), the 5 is the reddest. This profile is located in the highest relative position and occurs in a flat-sloped relief (Figure 7). The profiles 7 and 8 occurs in similar relative position (Figure 7B). However, the colors observed through them are different, which shows different processes in their formation. The profile 8 is the more yellowish profile. This characteristic is related to environments with low iron concentration, high water flux and, or, high organic matter content. These types of environments favor the goethite formation as it limits the Fe2+ availability for oxide formation (Schwertmann, 1993). The great thickness of the A horizon (0.30 m, Figure 6) and its dark color indicate that the organic matter content may be one of the main factors in this case. However, the flow of water received from the higher parts of the landscape certainly enhances the formation of goethite in this case.

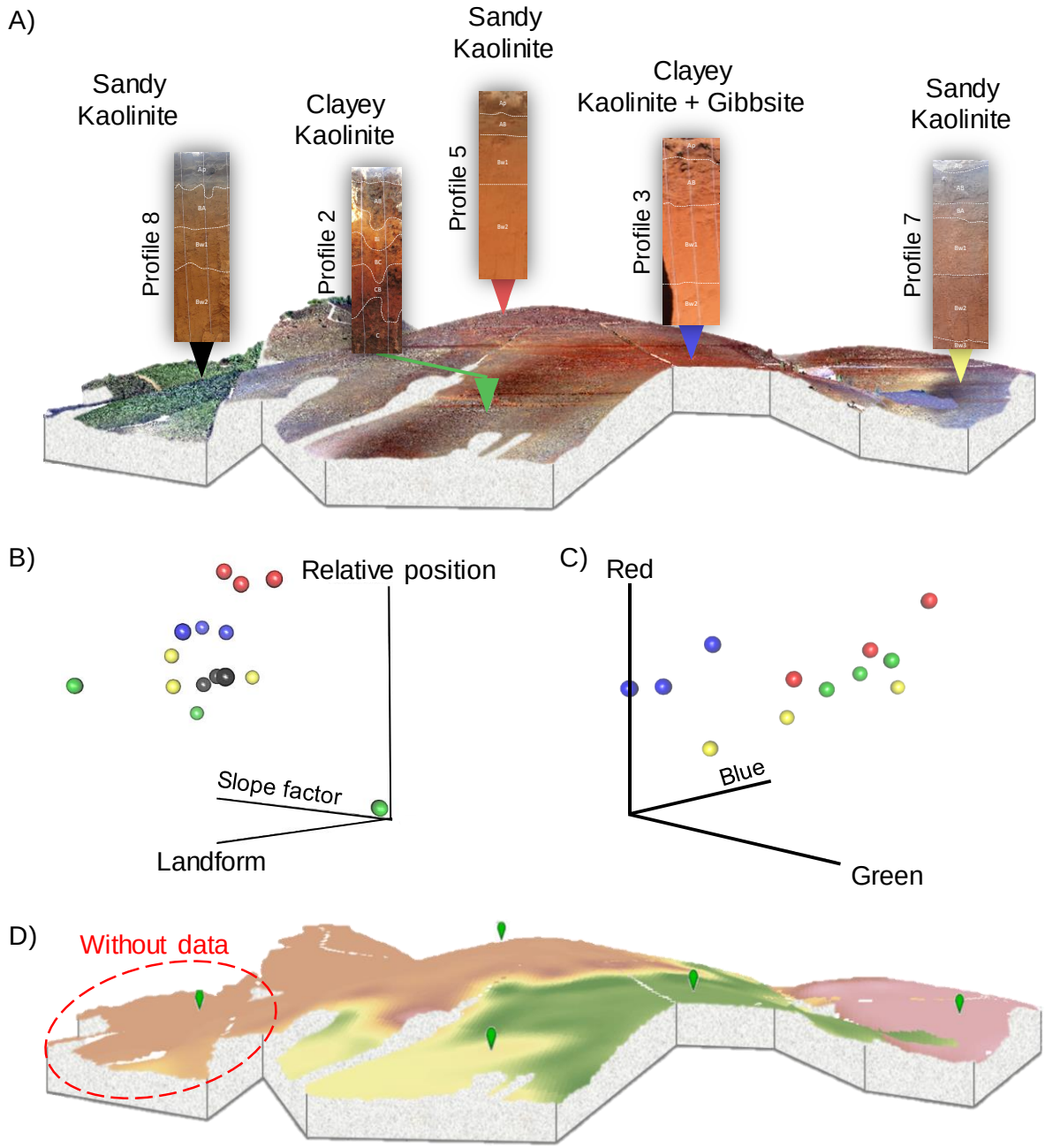

Figure 7. A) UAV image and soil profiles with characteristics inferred from proximal sensing; B) 3D plot of Principal component analysis from terrain derivatives; C) 3D plot of UAV RGB image; D) Spline based on grouping with RGB and terrain derivatives (UAV data) and its relationship with pedons.

1.4. CONCLUSIONS

a) The data from proximal sensors allows to make more robust hypothesis about soil formation processes.

b) The clusterization with high density sensor data allows to better describe soil profiles horizonation.

c) The Vis-NIR-SWIR spectral range relationship with soil color provides better correspondence with traditional field observation.

d) The combined use of Vis-NIR-SWIR, MIR and pXRF allows to identify the horizon boundaries more appropriately related to soil forming processes.

e) The variability through "homogeneous" Ferralsols profiles can be accessed by using portable spectroscopic and XRF sensors, which could allow to understand the polygenetic phases on soil profiles.

f) Surface data obtained with an Unnamed Aerial Vehicles (UAV) allows to better explain the soil bodies occurrence on the landscape.

g) The high spatial resolution of the UAV data associated to field sensors can be useful on real-time environment mapping at farm scale allowing to understand the soil forming process and behavior.

ACKNOWLEDGEMENTS

The authors would like to thank the Coordination of Superior Level Staff Improvement (CAPES) for providing PhD scholarship to the first author and to the São Paulo Research Foundation (FAPESP) for providing funds to the Thematic Project "Geotechnologies on a Detailed Digital Soil Mapping and the Brazilian Soil Spectral Library: Development and Applications" number 2014-22262-0. Special thanks to the Research Group "Geotechnologies in Soil Science" (GeoCiS: https://esalqgeocis.wixsite.com/geocis) for the support and always friendly relationships.

REFERENCES

AgiSoft PhotoScan Professional (Version 1.2.6) (Software). (2016*). Retrieved from http://www.agisoft.com/downloads/installer/

Alvares, C.A.; Stape, J.L.; Sentelhas, P.C.; Gonçalves, J.L.M. & Sparovek, G. 2013. Köppen's climate classification map for Brazil. Meteorologische Zeitschrift 22: 711-728.

Betard, F., 2012. Spatial variations of soil weathering processes in a tropical mountain environment: the Baturite massif and its piedmont (Ceara, NE Brazil). Catena 93, 18–28.

Bokhorst, M.P.; Beets, C.J.; Marković, S.B.; Gerasimenko, N.P.; Matviishina, Z.N.; Frechen, M. Pedo-chemical climate proxies in Late Pleistocene Serbian–Ukranian loess sequences. Quaternary International, Volume 198, Issues 1–2, 2009, Pages 113-123, ISSN 1040-6182 https://doi.org/10.1016/j.quaint.2008.09.003

Brinkman, R. 1970. Ferrolysis, a hydromorphic soil forming process. Geoderma 3:199–206.

Buol, S.W. TROPICAL SOILS. Humid Tropical, Editor(s): Daniel Hillel, Encyclopedia of Soils in the Environment, Elsevier, 2005, Pages 187-195, ISBN 9780123485304, https://doi.org/10.1016/B0-12-348530-4/00511-7.

Calinski, T., Harabasz, J. (1974): A dendrite method for cluster analysis. Communications in Statistics, 3, 1-27.

Campos, R. C., & Demattê, J. A. M.. (2004). Cor do solo: uma abordagem da forma convencional de obtenção em oposição à automatização do método para fins de classificação de solos. Revista Brasileira de Ciência do Solo, 28(5), 853-863. https://dx.doi.org/10.1590/S0100-06832004000500008

Conrad, Olaf & Bechtel, Benjamin & Dietrich, Helge & Fischer, Elke & Gerlitz, Lars & Wehberg, Jan & Wichmann, Volker & Böhner, Jürgen. (2015). System for Automated Geoscientific Analyses (SAGA) v. 2.1.4. Geoscientific Model Development. 8. 1991-2007. 10.5194/gmd-8-1991-2015.

Dasch, E.J., 1969. Strontium isotopes in weathering profiles, deep-sea sediments, and sedimentary rocks. Geochim. Cosmochim. Acta 33, 1521–1552. https://doi.org/10.1016/0016-7037(69)90153-7.

Demattê, J.A.M.; André Carnieletto Dotto, Ariane F.S. Paiva, Marcus V. Sato, Ricardo S.D. Dalmolin, Maria do Socorro B. de Araújo, Elisângela B. da Silva, Marcos R. Nanni, Alexandre ten Caten, Norberto C. Noronha, Marilusa P.C. Lacerda, José Coelho de Araújo Filho, Rodnei Rizzo, Henrique Bellinaso, Márcio R. Francelino, Carlos E.G.R. Schaefer, Luiz E. Vicente, Uemeson J. dos Santos, Everardo V. de Sá Barretto Sampaio, Rômulo S.C. Menezes, José João L.L. de Souza, Walter A.P. Abrahão, Ricardo M. Coelho, Célia R. Grego, João L. Lani, Antonio R. Fernandes, Deyvison A.M. Gonçalves, Sérgio H.G. Silva, Michele D. de Menezes, Nilton Curi, Eduardo G. Couto, Lúcia H.C. dos Anjos, Marcos B. Ceddia, Érika F.M. Pinheiro, Sabine Grunwald, Gustavo M. Vasques, José Marques Júnior, Airon J. da Silva, Marcos C. de Vasconcelos Barreto, Gabriel N. Nóbrega, Marcelo Z. da Silva, Sara F. de Souza, Gustavo S. Valladares, João Herbert M. Viana, Fabricio da Silva Terra, Ingrid Horák-Terra, Peterson R. Fiorio, Rafael C. da Silva, Elizio F. Frade Júnior, Raimundo H.C. Lima, José M. Filippini Alba, Valdomiro S. de Souza Junior, Maria De Lourdes Mendonça Santos Brefin, Maria De Lourdes P. Ruivo, Tiago O. Ferreira, Marny A. Brait, Norton R. Caetano, Idone Bringhenti, Wanderson de Sousa Mendes, José L. Safanelli, Clécia C.B. Guimarães, Raul R. Poppiel, Arnaldo Barros e Souza, Carlos A. Quesada, Hilton T. Zarate do Couto, The Brazilian Soil Spectral Library (BSSL): A general view, application and challenges, Geoderma, Volume 354, 2019, 113793, ISSN 0016-7061, https://doi.org/10.1016/j.geoderma.2019.05.043.

Desgraupes, B. (2018). clusterCrit: Clustering Indices. R package version 1.2.8. https://CRAN.R-project.org/package=clusterCrit.

Dixon, J.B. and Weed, S.B. (1989) Minerals in Soil Environments. 2nd Edition, Soil Science Society of America, Madison.

Fajardo, M., McBratney, A., Whelan, B., 2016. Fuzzy clustering of Vis–NIR spectra for the objective recognition of soil morphological horizons in soil profiles. 2015. Geoderma 263 (2016) 244–253. http://dx.doi.org/10.1016/j.geoderma.2015.05.010.

Fedo CM, Nesbitt HW, Young GM. Unravelling the effects of potassium metasomatism in sedimentary rocks and paleosols, with implications for paleoweathering conditions and provenance. Geology. 1995;23:921–924

Franke, R. 1982. Smooth Interpolation of Scattered Data by Local Thin Plate Splines. Computer and Mathematics with Applications. Vol. 8. No. 4. pp. 273–281. Great Britain.

Grauer-Gray, J., HarteminK, A. E., 2018. Raster sampling of soil profiles. Geoderma 318 (2018) 99–108. https://doi.org/10.1016/j.geoderma.2017.12.029

Harnois LUC. T h e CIW index: a new chemical index of weathering. Sediment Geol. 1988;55:319–322.

Hartemink, A.E., Minasny, B., 2014. Towards digital soil morphometrics. Geoderma 230–231 (2014) 305–317. http://dx.doi.org/10.1016/j.geoderma.2014.03.008.

Jayawardena, U.d.S., Izawa, E., 1994. A new chemical index of weathering for metamorphic silicate rocks in tropical regions: a study from Sri Lanka. Eng. Geol. 36, 303–310.

Jenny, H. (1941) Factors of Soil Formation: A System of Quantitative Pedology. Dover Publications, New York, 281 p.

Johnson, D. L. and D. Watson-Stegner. 1987. Evolution model of pedogenesis. Soil Sci. 143: 349–366.

Maechler, M., Rousseeuw, P., Struyf, A., Hubert, M., Hornik, K.(2018). cluster: Cluster Analysis Basics and Extensions. R package version 2.0.7-1.

Maynard, J., 1992. Chemistry of modern soils as a guide to interpreting Precambrian paleosols. The Journal of Geology 100, 279–289.

McBratney, A.B.; Mendonça Santos, M.L; Minasny, B. On digital soil mapping. Geoderma, Volume 117, Issues 1–2, 2003, Pages 3-52, ISSN 0016-7061, https://doi.org/10.1016/S0016-7061(03)00223-4.

McDaniel, P. A., R. W. Gabehart, A. L. Falen, J. E. Hammel, and R. J. Reuter. 2001. Perched water tables on Argixeroll and Fragixeralf hillslopes. Soil Sci. Soc. Am. J. 65:805–810.

Mezzalira, S. (1989). Os fósseis do Estado de São Paulo. São Paulo, Secretaria do Meio Ambiente/Instituto Geológico. 2.ed. Série Pesquisa. 142p.

Minasny, Budiman & Stockmann, Uta & Hartemink, Alfred & Mcbratney, Alex. (2016). Measuring and Modelling Soil Depth Functions. 10.1007/978-3-319-28295-4_14.

Muggler, C. C. and P. Buurman. 2000. Erosion, sedimentation and pedogenesis in a polygenetic oxisol sequence in Minas Gerais, Brazil. Catena 41: 3–17.

Nesbitt, H. W., Young, G. M., 1989. Formation and diagenesis of weathering profiles. The Journal of Geology 97, 129-147

Oliveira, J.B.; Prado, H. Carta pedológica semidetalhada do estado de São Paulo: folha de Piracicaba. Campinas: Instituto Agronômico, 1989. Mapa, escala 1:100.000.

Ruxton, B.P., 1968. Measures of the degree of chemical weathering of rocks. The Journal of Geology 76, 518–527.

Santos, H.G.; Jacomine PKT, Anjos LHC, Oliveira VA, Lumbreras JF, Coelho MR, Almeida JÁ, Araújo Filho, J. C., Oliveira JB; Cunha TJF. Sistema brasileiro de classificação de solos. 5ª. ed. rev. e ampl., 356 p. − Brasília, DF: Embrapa, 2018.

Schaetzl, R. J.; Anderson, S. Soils: genesis and geomorphology. New York, NY: Cambridge University press, 2005.

Schwertmann, U. 1993. Relations Between Iron Oxides, Soil Color, and Soil Formation. In: J. M. Bigham, E. J. Ciolkosz, editors, Soil Color, SSSA Spec. Publ. 31. SSSA, Madison, WI. p. 51-69. doi:10.2136/sssaspecpub31.c4

Silva, S. H. G., Hartemink, A. E., Teixeira, A. F. S., Inda, A. V., Guilherme, L. R. G., Curia, N., 2018. Soil weathering analysis using a portable X-ray fluorescence (PXRF) spectrometer in an Inceptisol from the Brazilian Cerrado. Applied Clay Science 162 (2018) 27–37. https://doi.org/10.1016/j.clay.2018.05.028.

Souza, A. B.; Demattê, J. A. M.; Mello, F. A. O.; Salazar, D. F. U.; Mendes, W. S.; Safanelli, J. L. Ratio of Clay Spectroscopic Indices and its approach on soil morphometry, Geoderma, Volume 357, 2020, 113963, ISSN 0016-7061, https://doi.org/10.1016/j.geoderma.2019.113963.

Stenberg, B. (2010). Effects of soil sample pretreatments and standardised rewetting as interacted with sand classes on Vis-NIR predictions of clay and soil organic carbon. Geoderma. 158, 15-22.

Stockmann, U., Cattle, S.R., Minasny, B., McBratney, A.B., 2016. Utilizing portable X-ray fluorescence spectrometry for in-field investigation of pedogenesis. Catena 139 (2016) 220–231. http://dx.doi.org/10.1016/j.catena.2016.01.007.

Terra, F. S.; Demattê, J. A. M.; Viscarra-Rossel, A. A. Spectral libraries for quantitative analyses of tropical Brazilian soils: Comparing vis–NIR and mid-IR reflectance data, Geoderma, Volumes 255–256, 2015, Pages 81-93, ISSN 0016-7061, https://doi.org/10.1016/j.geoderma.2015.04.017.

Terra, F.S., Demattê, J.A.M., Rossel, R.A.V., 2018. Proximal spectral sensing in pedological assessments: vis–NIR spectra for soil classification based on weathering and pedogenesis. Geoderma 318 (2018) 123–136. https://doi.org/10.1016/j.geoderma.2017.10.053.

van Breemen N, Buurman P. Soil formation. 2nd ed. Dordrecht: Kluwer Academic Publishers, 2002.

van Ranst, E., Coninck, F., 2002. Evaluation of ferrolysis in soil formation. Eur. J. Soil Sci. 53, 513-519. https://doi.org/10.1046/j.1365-2389.2002.00475.x

Viscarra-Rossel, R. A.; Cattle, S. R.; Ortega, A; Fouad, Y In situ measurements of soil colour, mineral composition and clay content by vis–NIR spectroscopy, Geoderma, Volume 150, Issues 3–4, 2009, Pages 253-266, ISSN 0016-7061, https://doi.org/10.1016/j.geoderma.2009.01.025.

Viscarra-Rossel, R.A., Walvoort, D. J.J., Mcbratney, A.B., Janik, L.J. & Skjemstad, J.O. 2006. Visible, near infrared, mid infrared or combined diffuse reflectance spectroscopy for simultaneous assessment of various soil properties. Geoderma, Amsterdam, v. 131, n. 1/2, p. 59–75.

Viscarra-Rossel, R.A.; Behrens, T.; Ben-Dor, E; Brown, D.J.; Demattê, J.A.M.; Shepherd, K.D.; Shi, Z.; Stenberg, B.; Stevens, A.; Adamchuk, V.; Aïchi, H.; Barthès, B.G.; Bartholomeus, H.M.; Bayer, A.D.; Bernoux, M.; Böttcher, K.; Brodský, L.; Du, C.W.; Chappell, A.; Fouad, Y.; Genot, V.; Gomez, C.; Grunwald, S.; Gubler, A.; Guerrero, C.; Hedley, C.B.; Knadel, M.; Morrás, H.J.M.; Nocita, M.; Ramirez-Lopez, L.; Roudier, P.; Rufasto Campos, E.M; Sanborn, P.; Sellitto, V.M.; Sudduth, K.A.; Rawlins, B.G.; Walter, C.; Winowiecki, L.A.; Hong, S.Y.; Ji, W. A global spectral library to characterize the world's soil, Earth-Science Reviews, Volume 155, 2016, Pages 198-230, ISSN 0012-8252, https://doi.org/10.1016/j.earscirev.2016.01.012.

Weindorf, D.C., Bakr, N., Zhu, Y., 2014. Advances in Portable X-ray Fluorescence (PXRF) for environmental, pedological, and agronomic applications. Adv. Agron. 128, 1–45.

Weindorf, D.C., Zhu, Y., Haggard, B., Lofton, J., Chakraborty, S., Bakr, N., Zhang, W., Weindorf, W.C., Legoria, M., 2012a. Enhanced Pedon Horizonation Using Portable X-ray Fluorescence Spectrometry. Soil Sci. Soc. Am. J: Volume 76: Number 2. doi:10.2136/sssaj2011.0174.

Weindorf, D.C., Zhu, Y., McDaniel, P., Valerio, M., Lynn, L., Michaelson, G., Clark, M., Ping, C.L., 2012b. Characterizing soils via portable x-ray fluorescence spectrometer: 2. Spodic and Albic horizons. Geoderma 189–190, 268–277. doi:10.1016/j.geoderma.2012.06.034.

Wickham, H. The Split-Apply-Combine Strategy for Data Analysis. Journal of Statistical Software, 2011, 40(1), 1-29.

World Reference Base for Soil Resources - WRB: A framework for international classification, correlation and communication. Food and Agriculture Organization of the United Nations. Rome: IUSS/ISRIC/FAO; 2014. (World soil resources reports, 106)

Zhang, Y., Hartemink, A. E. Soil horizon delineation using vis-NIR and pXRF data, CATENA, Volume 180, 2019a, Pages 298-308, ISSN 0341-8162, https://doi.org/10.1016/j.catena.2019.05.001.

Zhang, Y., Hartemink, A.E., 2019c. A method for automated soil horizon delineation using digital images. Geoderma 343, 97–115.

2. SOIL PROFILE HETEROGENEITY AND ITS VARIATION ALONG THE LANDSCAPE: AN SENSORS BASED APPROACH

ABSTRACT

The technological and computational development has given new possibilities for soil scientist to describe and infers about soil development and functions. Why not try classify soil horizons or profiles according to its spectral signature, elements abundance profiles or others sensors information available nowadays? We proposed to study the soil profile heterogeneity by using reflectance (Vis-NIR-SWIR and MIR), X-Ray Fluorescence and magnetic susceptibility aiming to quantify it with the proposed "Profile Heterogeneity Index" (PHI) through seven topossequences in a complex area. The main hypotheses are the following: i) The differences between consecutive layers can be expressed by the sensors; ii) The PHI are higher on the transitions between geologic material and on the middle slope due to the mass flux; iii) The sensors have different capabilities to identify contrasts between layers. Twenty-seven points were sampled through seven topossequences in a 165 ha farm, in Rio das Pedras municipality, SP, Brazil. The samples were dried and sifted and submitted to Vis-NIR-SWIR and MIR reflectance analyses and to pXRF and to a Magnetic Susceptibilimeter. The differences between two consecutive layers were calculated by subtracting the bottom data from the above one ("Surface" – "Undersurface") for all data sets. The results were shown as a depth function with proportional colors to highlight the heterogeneity through the soil profile. This approach allows to identify where the differences occurs and allows to develop hypothesis about soil forming factors and processes. A Profile Heterogeneity index (PHI) was proposed to quantify the differences between layers in a given profile. The differences between two consecutive layers are well expressed by subtracting their sensor data. Despite of PHI, this approach is indispensable to completely understand the soil heterogeneity inside of a given soil profile when using sensors. The subtraction of data from consecutive layers is a way to highlight the contrasts on soil profiles which allows to identify transitions that can be related to material transportation/deposition or processes associated to climate legacy. The PHI reduces the information due to be calculated as a mean of the contrasts between layers and is more effective on abrupt transitions. The greater PHI were mainly related to material deposition through the landscape and to geologic contrasting materials. The sensors give complementary information to the profile heterogeneity characterization.

Keywords: Profile Heterogeneity Index; Diffuse Reflectance; Vis-NIR-SWIR; MIR; pXRF; landscape

2.1. INTRODUCTION

The soil profile organization is a registry of its development processes which can inform about its attributes and behavior on the landscape (Schaetzl and Anderson, 2005). The water dynamics drives the soil genesis processes and determine its capabilities on environmental functions and for agricultural applications.

Soil classification systems have been developed around the word trying to facilitate the communication and understanding of soil profiles (WRB, 2014). However, most of the systems are based on traditional ways to describe soil bodies which could limit the understanding and the applications of the surveys. The soil surveys are based on recognize patterns through the landscape and describe it on trenches. These observations allow to make inferences about the soil properties. However, the current ways are time consuming, cost limiting and does not give the full information about the pedon.

The technological and computational development has given new possibilities for soil scientist to describe and infers about soil development and functions. The reflectance (Viscarra-Rossel et al., 2016), X-Ray fluorescence (XRF) (Weindorf et al., 2012, 2013) and magnetic susceptibility (MS) (Kanu et al., 2019; Jordanova et al., 2019; Asgaria et al., 2018; Fine et al., 1992) are among the main ones.

The reflectance spectroscopy through Visible, Near, Shortwave and Middle Infrared have been used to estimate several soil properties successfully by using chemometric technics (Viscarra-Rossel, 2016). These technics are based on electron transitions and molecular vibrations with a wide range of possibilities from micro to regional and world scale. The organic matter and mineralogical assemblies are the main spectrally active soil compounds. Several spectral libraries have been developed in the world to understand soil spectral signatures (Demattê et al., 2019; Viscarra-Rossel et al., 2016).

Together with these approaches, the X-ray fluorescence have been used to accesses the elements abundance on soil studies (Sun et al., 2020; Zhang and Hartemink, 2019). This is a powerful tool based on specific electronic transitions induced by an X-ray source and can be used even on field measurements (portable XRF) (Stockmann et al., 2016). The magnetic susceptibility can provide information about the soil mineralogy, texture and other soil attributes (Fine et al., 1992; Camargo et al., 2016; Asgaria et al., 2018; Kanu). This property is important on the study of soil parent materials and is associated mainly to pedogenetic formation of ferrimagnetic minerals as the maghemite (Asgaria et al., 2018).

Despite of this, the soil organization was lost on this process once it was not taken into account the horizonation and its context on the landscape. The contrasts between consecutive layers defines the vertical water flow and the nutrients dynamics. Also, the erodibility and conservation practices are determined by the soil vertical organization together with its context on the landscape. Some efforts have been made on this way. Sun et al. (2020) studied

pXRF to describe argillic and calcic horizons. Zhang and Hartemink (2019) used Vis-NIR and pXRF data for horizon delineation. Demattê et al. (2014) studding reflectance proposed the MIRs method to evaluate the differences between samples related to the soil classification. However, we must to develop ways to use the denser information provided by the equipment. Why not classify soil horizons or profiles according to its spectral signature, elements abundance profiles or others information available nowadays?

In this context, we proposed to study the soil profile heterogeneity by using reflectance (Vis-NIR-SWIR and MIR), X-Ray Fluorescence and magnetic susceptibility aiming to quantify it with the proposed "Profile Heterogeneity Index" (PHI) through seven topossequences in a complex area. The main hypotheses are the following: i) The differences between consecutive layers can be expressed by the sensors; ii) The PHI are higher on the transitions between geologic material and on the middle slope due to the mass flux; iii) The sensors have different capabilities to identify contrasts between layers.

2.2. MATERIAL AND METHODS

The research was conducted in a 165 ha farm, in Rio das Pedras municipality, SP, Brazil (Figure 1a). The elevation range is around 100 m and the parent materials are highly diverse, mainly Basaltic from Serra Geral Formation (KSg) and Sedimentary rocks from Tatuí (Ptt) and Iratí (Pi) formations (Mezzalira, 1989) (Figure 1b).

Twenty-seven points were sampled through seven topossequences (Figure 1a). Eleven samples were collected on each point: one from surface and 10 from undersurface (Figure 1c). The undersurface samples were collected every 0.10 m until 1 m depth with an auger. The material was disposed on a graduated canvas to soil profile simulation and for later packaging. The samples were dried (45 ºC) and sifted (2 mm) and submitted to a spectroradiometer working on the 350 - 2,500 nm range, to another working on 2,500 - 25,00 nm, to a portable X-Ray Fluorescence and to a susceptibilimeter to measure the magnetic susceptibility (Figure 1d).

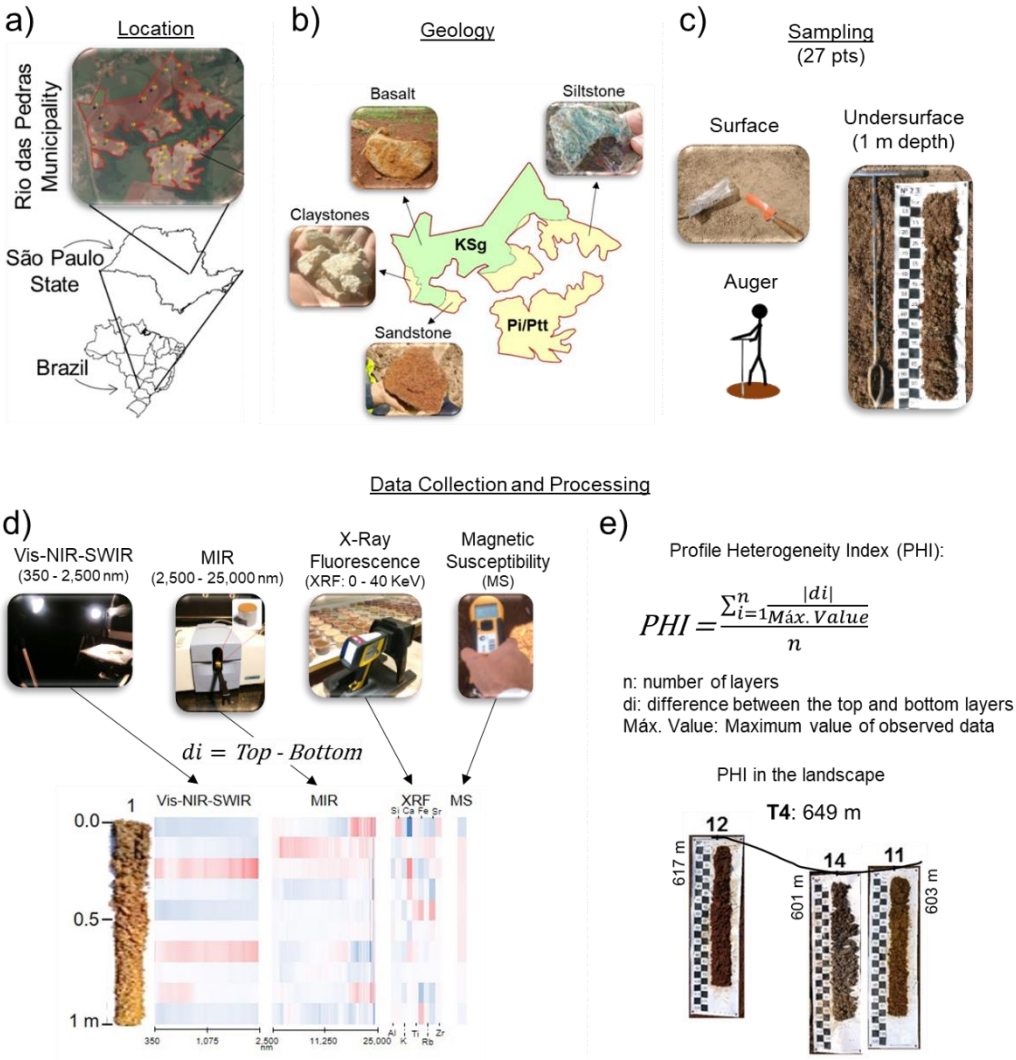

Figure 1. Study flowchart: a) study area and points of collection; b) geologic formations and parent materials found in the area; c) Sampling methods; d) sensors, data acquisition and heterogeneity soil profile; e) profile heterogeneity index and the landscape contexts.

The Vis-NIR-SWIR spectra were registered by a FieldSpec 3 spectroradiometer (Analytical Spectral Devices, ASD, Boulder, CO), which has a spectral range from 350 to 2,500 nm. The spectral resolution varies for each spectral range, as follows: 1 nm, from 350 to 700 nm; 3 nm, from 700 to 1,400 nm; and 10 nm from 1,400 to 2,500 nm. However, the output data were resampled to 1 nm, resulting in 2,151 channels (Demattê et al., 2019). A white spectral plate was used as a maximum reflectance reference.

The soil samples were sieved to 100 mesh, disposed in a bucket, smoothed with a spatula and submitted to a Diffuse Reflectance Infra-Red Fourier Transformed (DRIFT) in the

Middle Infrared (MIR) range (2,500 to 25,000 nm) (Figure 1d). The data from each sample were obtained with 32 readings with 2 cm^{-1} channel width resampled to 1 cm^{-1}, totalizing 3,432 channels. Each wavenumber (cm^{-1}) were transformed to wavelength (nm) dividing by 10.000.000. A gold plate was used as reference for the maximum reflectance for every profile.

A portable X-Ray Fluorescence (pXRF) was used to measure the elemental concentration on the dry-sifted samples (Figure 1d). This equipment works with a Silver anode (Ag) X-Ray tube (4 W) in the range from 0 to 40 keV. Calibration was checked by using the NIST 316 alloy, two standard soil samples (SRM 2710a – Montana I Soil; and SRM 2711a – Montana II Soil) and a pure SiO_2 sample, both from NIST. It was used two energy beans to optimize the light elements estimation: 0 to 10 keV and 0 to 40 keV. This procedure (0 to 10 keV) improves the signal/noise ratio allowing to get better estimations once high energy scattering increases the noise at low energy channels. The equipment was used on "Soil" mode, which is an internal software that allows to estimate the elements concentration in soil-like matrices. The pXRF interacts with matter in an atomic level reporting the chemical composition of the sample for elements with atomic number above 11 (Stockmann et al., 2016). This is a primary method based on direct interactions between X-ray energy and elements so it can provide relative elemental concentration of the samples (Weindorf and Chakraborty, 2014).

The MS was assessed with a KT-10, that measures the susceptibility that a given sample has to be magnetized by induction (Figure 1d), which depends on its composition and is mainly associated to the Fe and clay contents (Kanu et al., 2019). The "zero" susceptibility was registered in the air.

The differences between two consecutive layers were calculated by subtracting the bottom data from the above one ("Surface" – "Undersurface") for all data sets. The results were shown as a depth function with proportional colors to highlight the heterogeneity through the soil profile. This approach allows to identify where the differences occurs and allows to develop hypothesis about soil forming factors and processes.

A Profile Heterogeneity index (PHI) was proposed to quantify the differences between layers (Fig. 1e). This index is a mean of the module normalized differences on the soil profile. A homogeneous profile will trend to a PHI equals "zero" while a highly heterogeneous one will trend to PHI equals "One". This index can be used for every data type and collecting

resolution. In fact, the expected differences even through the homogeneously soil types, like Ferralsols, are reduced once it considers subsequent layers.

2.3. RESULTS AND DISCUSSION

The profile heterogeneity indices (PHI) were effectives on showing the contrasts inside of each soil profile (Table 1). The depth functions with the differences between two consecutive layers also were very informative through the soil profile (Figure 2 and 3). In fact, these information complements each other. The PHI shows a superficial data once it represents a compilation of the contrasts inside of a given profile. The depth functions must to be used to identify where and why is the contrast occurring between the layers.

One of the most evident result was that the reflectance from surface was greater than that from the 0 - 0.10 m layer in most cases (Figure 2 and 3). The segregation and selective transportation are the main processes associated to this fact. Sand accumulation and the loss of clay results on a greater reflectance. This fact is important on soil studies once the surface reflectance is commonly used to estimate soil properties by using satellite data. However, in the profiles 22 and 24 the reflectance from surface was less intense than that from undersurface (Figure 3, Vis-NIR-SWIR). This fact could be associated to the presence of opaque minerals on the sand fraction or even to the organic matter content.

The PHI from Vis-NIR-SWIR data varied between 0.06 (profiles 24 and 26) and 0.16 (profiles 9 and 11) (Table 1). The more homogeneous ones (profiles 24 and 26) developed from sedimentary rocks, while the profiles 9 and 11 developed above basaltic parent material. Soil bodies that develops on sedimentary rocks are commonly more homogenous concerning the mineralogical assembly since it has already gone through several weathering cycles. The opposite can be observed on the mafic rocks. In this case, the landform plays an important role on driving the water dynamics, such as accumulation and leaching processes. In fact, basaltic materials can be strongly modified by weathering under tropical conditions due to its primary minerals contents. The evidences of this differentiation can be seen on the topossequences 4, mainly due to the contrasting colors (Figure 4). Zhang and Hartemink (2019) studied Vis-NIR and pXRF data for soil horizon delineation by clustering analyses. They observed that the color plays an important role on identifying A horizons while the weathering indices from pXRF does to the B horizons.

The magnetic susceptibility PHI ranges from 0.02 (profile 6) to 0.25 (profile 27). There is here an interesting property of the PHI. The use of the maximum value of a given attribute to standardize the PHI range for each profile highlighted the differences on the specific scale to each soil profile. In other words, the same difference in the content of some element can be more significant in one profile than in another. Due to this fact, the soil profiles developed from sedimentary rocks (which have much less ferromagnetic minerals than those developed from basaltic rocks) showed higher values to the PHI.

The profile 6 developed from basaltic material from and highlighted the material deposited by the mass flow in the landscape (profiles 3, 7 and 9, for example) and that accumulated due the selective transportation (profile 2).

Table 1. Profile heterogeneity indices (PHI).

Profile	Vis-NIR-SWIR	MIR	XRF									MS
			Al	Si	K	Ca	Ti	Fe	Rb	Sr	Zr	
1	0.10	0.09	0.06	0.09	0.09	0.24	0.07	0.19	0.08	0.20	0.05	0.08
2	0.12	0.08	0.03	0.05	0.00	0.15	0.06	0.06	0.32	0.06	0.04	0.06
3	0.09	0.08	0.08	0.08	0.04	0.15	0.07	0.06	0.05	0.12	0.04	0.10
4	0.11	0.09	0.06	0.07	0.00	0.25	0.05	0.03	0.39	0.06	0.04	0.04
5	0.08	0.08	0.04	0.07	0.25	0.11	0.06	0.05	0.11	0.09	0.04	0.03
6	0.08	0.12	0.07	0.05	0.00	0.20	0.04	0.04	0.55	0.12	0.05	0.02
7	0.09	0.09	0.06	0.05	0.06	0.18	0.08	0.10	0.05	0.18	0.07	0.13
8	0.14	0.08	0.05	0.05	0.08	0.33	0.03	0.05	0.06	0.13	0.07	0.05
9	0.16	0.08	0.10	0.08	0.05	0.21	0.04	0.06	0.05	0.09	0.05	0.13
10	0.11	0.08	0.13	0.08	0.08	0.11	0.10	0.07	0.07	0.06	0.08	0.11
11	0.16	0.08	0.07	0.07	0.11	0.20	0.09	0.09	0.11	0.06	0.08	0.13
12	0.08	0.08	0.10	0.13	0.00	0.19	0.10	0.11	0.41	0.20	0.13	0.06
13	0.10	0.07	0.08	0.08	0.00	0.25	0.03	0.04	0.74	0.21	0.05	0.05
14	0.12	0.07	0.07	0.06	0.08	0.20	0.04	0.10	0.08	0.10	0.05	0.10
15	0.09	0.07	0.08	0.10	0.00	0.16	0.04	0.04	0.35	0.08	0.07	0.06
16	0.10	0.08	0.07	0.05	0.08	0.16	0.08	0.08	0.07	0.15	0.10	0.12
17	0.08	0.08	0.07	0.07	0.08	0.19	0.09	0.14	0.15	0.09	0.11	0.14
18	0.09	0.07	0.05	0.05	0.07	0.22	0.08	0.09	0.07	0.09	0.08	0.10
19	0.08	0.09	0.07	0.06	0.08	0.21	0.11	0.11	0.08	0.14	0.07	0.14
20	0.10	0.08	0.08	0.08	0.07	0.22	0.05	0.11	0.06	0.08	0.09	0.17
21	0.07	0.07	0.06	0.06	0.05	0.07	0.05	0.07	0.06	0.05	0.04	0.10
22	0.14	0.07	0.06	0.07	0.09	0.15	0.07	0.12	0.08	0.09	0.08	0.13
23	0.09	0.09	0.06	0.08	0.08	0.19	0.06	0.08	0.07	0.08	0.07	0.11
24	0.06	0.08	0.11	0.09	0.09	0.26	0.08	0.13	0.10	0.11	0.06	0.11
25	0.09	0.09	0.06	0.07	0.07	0.13	0.08	0.08	0.06	0.07	0.09	0.18
26	0.06	0.07	0.06	0.07	0.11	0.06	0.09	0.07	0.09	0.07	0.13	0.08
27	0.08	0.09	0.07	0.04	0.08	0.06	0.07	0.07	0.07	0.04	0.09	0.25

MIR: Middle infra-red; XRF: X-Ray fluorescence; MS: Magnectic susceptibility.

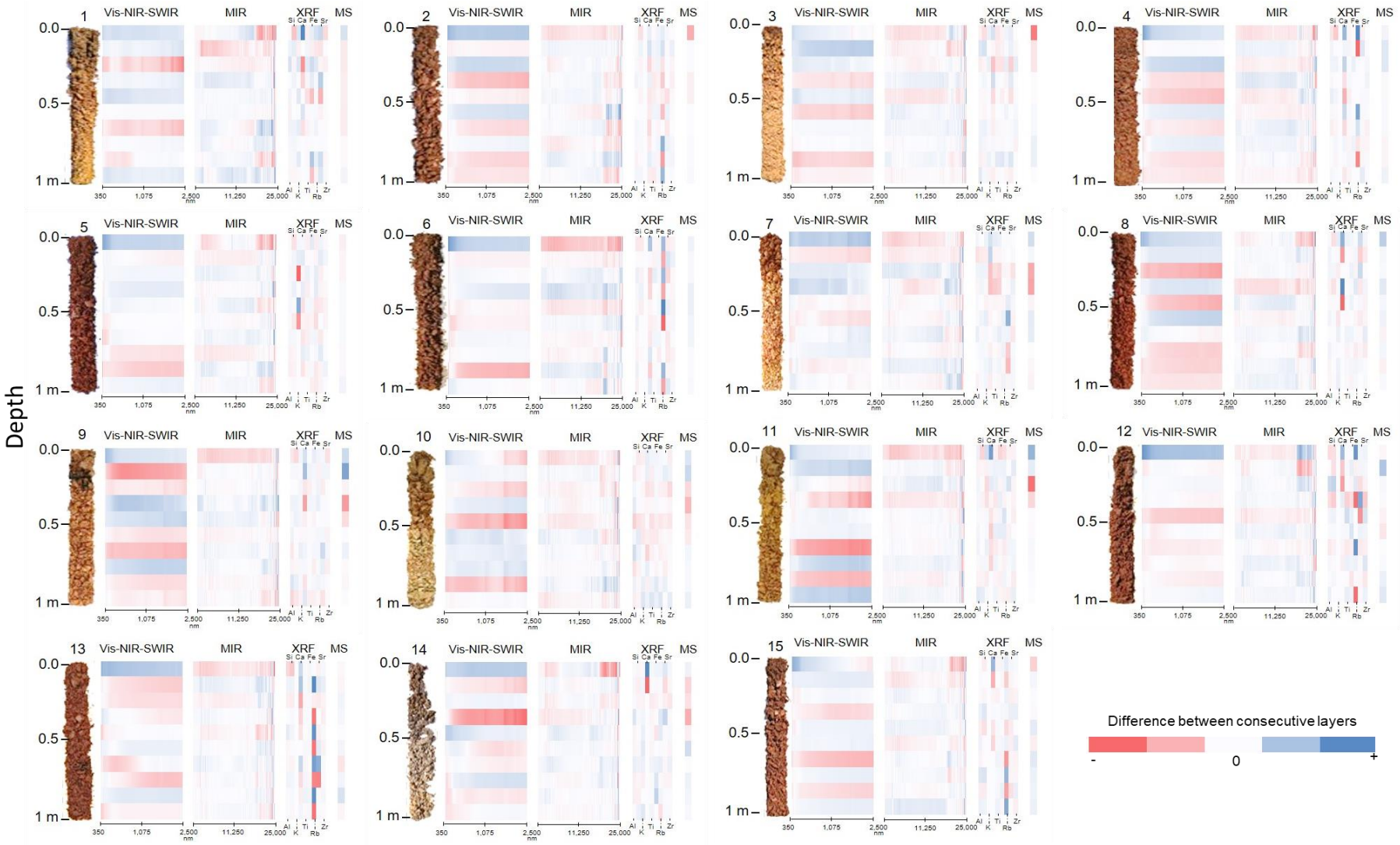

Figure 2. Soil profiles heterogeneity based on sensors. Profile 1 to 15.

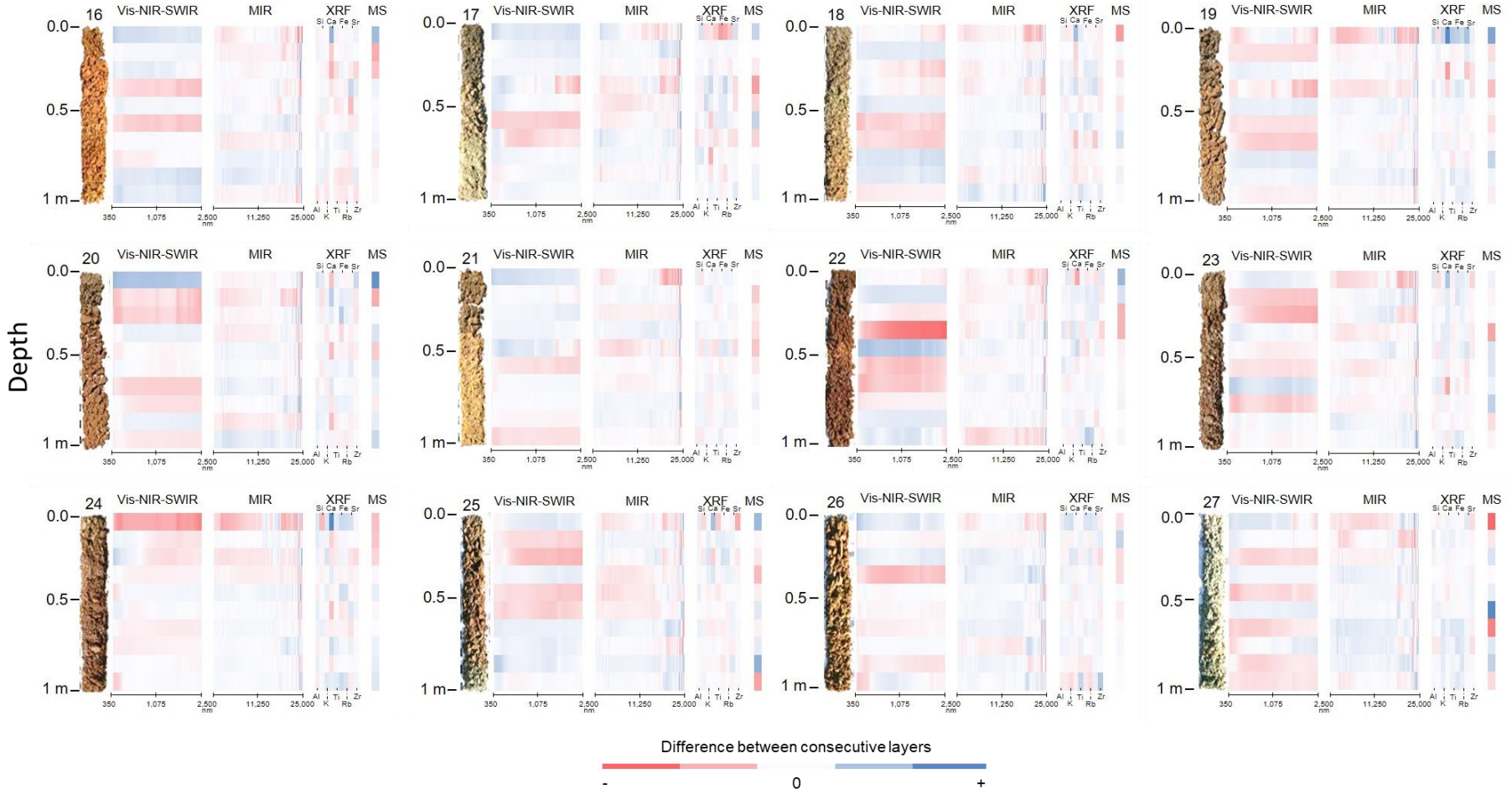

Figure 3. Soil profile heterogeneity based on sensor. Profile 16 to 27.

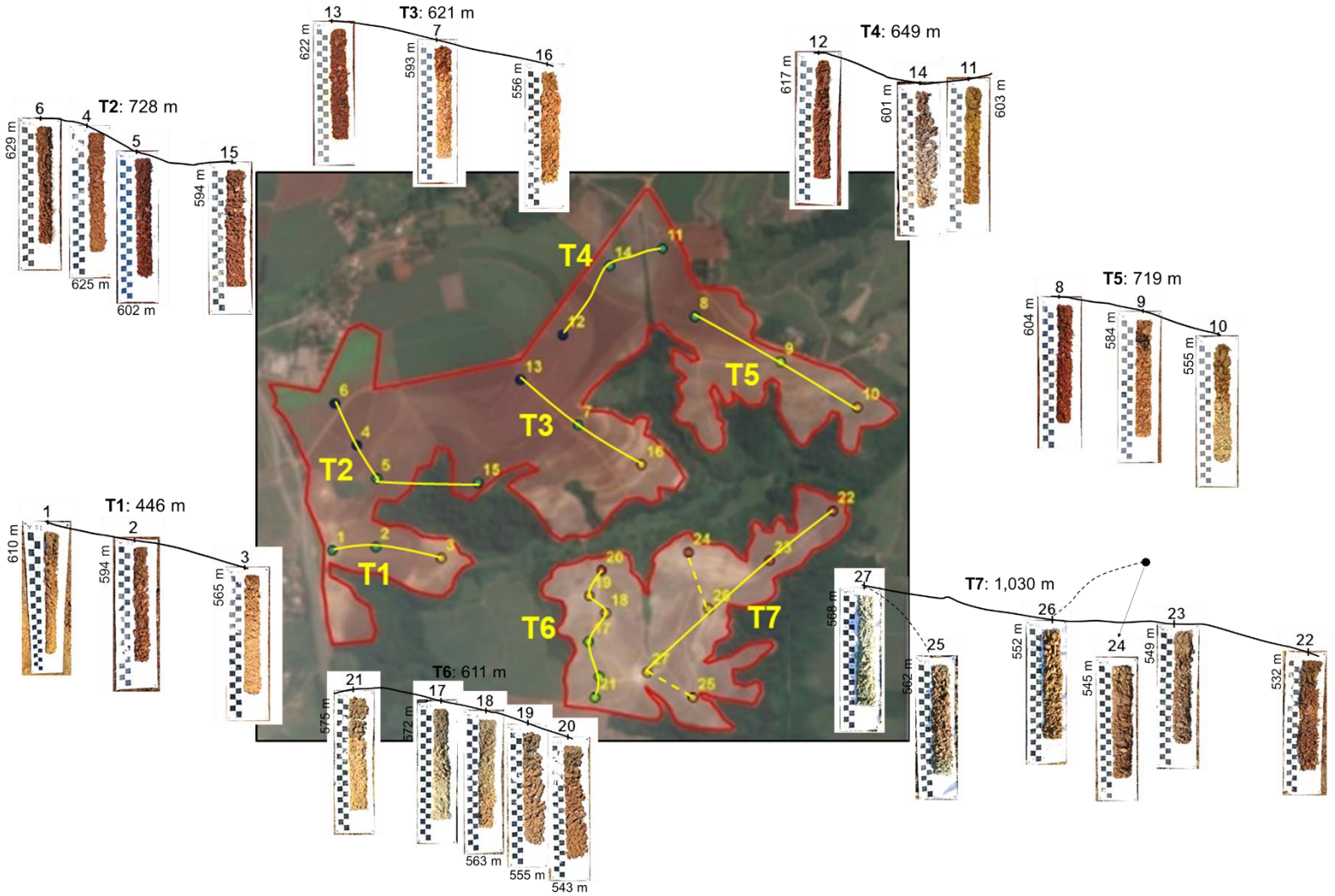

Figure 4. Soil profiles and its location on the landscape. The elevation and the topossequences (T1-T7) length are shown.Al

2.4. CONCLUSIONS

a) The differences between two consecutive layers are well expressed by subtracting their sensor data. Despite of PHI, this approach is indispensable to completely understand the soil heterogeneity inside of a given soil profile when using sensors.
b) The subtraction of data from consecutive layers is a way to highlight the contrasts on soil profiles which allows to identify transitions that can be related to material transportation/deposition or processes associated to climate legacy.
c) The PHI reduces the information due to be calculated as a mean of the contrasts between layers and is more effective on abrupt transitions.
d) The greather PHI were mainly related to material deposition through the landscape and to geologic contrasting materials.
e) The sensors give complementary information to the profile heterogeneity characterization.

ACKNOWLEDGEMENTS

We are grateful to Geotechnologies in Soil Science Group (GeoCiS/ESALQ-USP; http://esalqgeocis.wixsite.com/english) for team support. We also thank the anonymous reviewers to improve this paper. The MSc scholarship of the first author was provided by the National Council for Scientific and Technological Development (CNPq). Funding was provided by São Paulo Research Foundation (FAPESP, grant numbers 2014/22262-0, 2016/26124-6, and 2016/01597-9).

REFERENCES

Demattê, J.A.M.; André Carnieletto Dotto, Ariane F.S. Paiva, Marcus V. Sato, Ricardo S.D. Dalmolin, Maria do Socorro B. de Araújo, Elisângela B. da Silva, Marcos R. Nanni, Alexandre ten Caten, Norberto C. Noronha, Marilusa P.C. Lacerda, José Coelho de Araújo Filho, Rodnei Rizzo, Henrique Bellinaso, Márcio R. Francelino, Carlos E.G.R. Schaefer, Luiz E. Vicente, Uemeson J. dos Santos, Everardo V. de Sá Barretto Sampaio, Rômulo S.C. Menezes, José João L.L. de Souza, Walter A.P. Abrahão, Ricardo M. Coelho, Célia R. Grego, João L. Lani, Antonio R. Fernandes, Deyvison A.M. Gonçalves, Sérgio H.G. Silva, Michele D. de Menezes, Nilton Curi, Eduardo G. Couto, Lúcia H.C. dos Anjos, Marcos B. Ceddia, Érika F.M. Pinheiro, Sabine Grunwald, Gustavo M. Vasques, José Marques Júnior, Airon J. da Silva, Marcos C. de Vasconcelos Barreto, Gabriel N. Nóbrega, Marcelo Z. da Silva, Sara F. de Souza, Gustavo S. Valladares, João Herbert M. Viana, Fabricio da Silva Terra, Ingrid Horák-Terra, Peterson R. Fiorio, Rafael C. da Silva, Elizio F. Frade Júnior, Raimundo H.C. Lima, José M. Filippini Alba, Valdomiro S. de Souza Junior, Maria De Lourdes Mendonça Santos Brefin, Maria De Lourdes P. Ruivo, Tiago O. Ferreira, Marny A. Brait, Norton R. Caetano, Idone Bringhenti, Wanderson de Sousa Mendes, José L. Safanelli, Clécia C.B. Guimarães, Raul R. Poppiel, Arnaldo Barros e Souza, Carlos A. Quesada, Hilton T. Zarate do Couto, The Brazilian Soil Spectral Library (BSSL): A general view, application and challenges, Geoderma, Volume 354, 2019, 113793, ISSN 0016-7061, https://doi.org/10.1016/j.geoderma.2019.05.043.

Fujun Sun, Noura Bakr, Tommy Dang, Vung Pham, David C. Weindorf, Zhuodong Jiang, Hualei Li, Qiu-Bing Wang, Enhanced soil profile visualization using portable X-ray fluorescence (PXRF) spectrometry, Geoderma, Volume 358, 2020, 113997, ISSN 0016-7061, https://doi.org/10.1016/j.geoderma.2019.113997.

L. A. Camargo J. Marques Jr. G. T. Pereira L. R. F. Alleoni A. S. R. de S. Bahia D. De B. Teixeira, Pedotransfer functions to assess adsorbed phosphate using iron oxide content and magnetic susceptibility in an Oxisol, 2016, Volume32, Issue2, Pages 172-182Soil Use and Management, https://doi.org/10.1111/sum.12255

M. O. Kanu, O. C. Meludu, N. Basavaiah, A. S. Oniku, Relationship between mineral magnetic properties and soil textural parameters, 2019, Acta Geophysica, Volume 67, Issue 2, pp 517–532, https://doi.org/10.1007/s11600-019-00248-8

Mezzalira, S. (1989). Os fósseis do Estado de São Paulo. São Paulo, Secretaria do Meio Ambiente/Instituto Geológico. 2.ed. Série Pesquisa. 142p.

Najmeh Asgaria, Shamsollah Ayoubia,∗, Jose A.M. Demattê. Soil drainage assessment by magnetic susceptibility measures in western Iran, 2018, Geoderma Regional 13 (2018) 35–42. https://doi.org/10.1016/j.geodrs.2018.03.003

Renata Andrade, Wilson Missina Faria, Sérgio Henrique Godinho Silva, SomsubhraChakraborty, David C. Weindorf, Luiz Felipe Mesquita, Luiz Roberto Guimarães Guilherme, Nilton Curi, Predictionofsoilfertility via portable X-rayfluorescence (pXRF) spectrometryandsoiltexture in theBrazilianCoastalPlains, Geoderma, Volume 357, 2020, 113960, ISSN 0016-7061, https://doi.org/10.1016/j.geoderma.2019.113960.

Schaetzl, R. J.; Anderson, S. Soils: genesis and geomorphology. New York, NY: Cambridge University press, 2005.

U. Stockmann, S.R. Cattle, B. Minasny, Alex B. McBratney, Utilizing portable X-ray fluorescence spectrometry for in-field investigation of pedogenesis,CATENA,Volume 139,2016,Pages 220-231,ISSN 0341-8162,https://doi.org/10.1016/j.catena.2016.01.007.

Viscarra-Rossel, R.A.; Behrens, T.; Ben-Dor, E; Brown, D.J.; Demattê, J.A.M.; Shepherd, K.D.; Shi, Z.; Stenberg, B.; Stevens, A.; Adamchuk, V.; Aïchi, H.; Barthès, B.G.; Bartholomeus, H.M.; Bayer, A.D.; Bernoux, M.; Böttcher, K.; Brodský, L.; Du, C.W.; Chappell, A.; Fouad, Y.; Genot, V.; Gomez, C.; Grunwald, S.; Gubler, A.; Guerrero, C.; Hedley, C.B.; Knadel, M.; Morrás, H.J.M.; Nocita, M.; Ramirez-Lopez, L.; Roudier, P.; Rufasto Campos, E.M; Sanborn, P.; Sellitto, V.M.; Sudduth, K.A.; Rawlins, B.G.; Walter, C.; Winowiecki, L.A.; Hong, S.Y.; Ji, W. A global spectral library to characterize the world's soil, Earth-Science Reviews, Volume 155, 2016, Pages 198-230, ISSN 0012-8252, https://doi.org/10.1016/j.earscirev.2016.01.012.

WEINDORF, D. C.; CHAKRABORTY, S. Portable X-ray fluorescence spectrometry analysis of soils. Methods of Soil Analysis, v.1, n.1, 2016.

World Reference Base for Soil Resources - WRB: A framework for international classification, correlation and communication. Food and Agriculture Organization of the United Nations. Rome: IUSS/ISRIC/FAO; 2014. (World soil resources reports, 106)

Yakun Zhang, Alfred E. Hartemink, Soil horizon delineation using vis-NIR and pXRF data, CATENA, Volume 180, 2019, Pages 298-308, ISSN 0341-8162, https://doi.org/10.1016/j.catena.2019.05.001.

Yuanda Zhu, David C. Weindorf, Wentai Zhang, Characterizing soils using a portable X-ray fluorescence spectrometer: 1. Soil texture,Geoderma,Volumes 167–168,2011,Pages 167-177,ISSN 0016-7061,https://doi.org/10.1016/j.geoderma.2011.08.010.

3. SOIL SURFACE REFLECTANCE: WHAT ARE WE MISSING WHEN USING SATELLITE DATA?

ABSTRACT

The use of satellite data on the estimation of soil attributes is wide spread worldwide. However, what is the potential of this data on the estimation of weathering indices? How much is its performance affected by the mixing and by the data resolution? The main objectives on this work were: i) to show the difference of spectral signature between prepared and field conditions samples; ii) to compare the convoluted data from laboratory spectroradiometer with the spectral signatures from Sentinel and Landsat satellites; iii) to build models to predict soil weathering indices with both diffuse reflectance from samples under natural conditions, dry-sifted samples and from satellite images. Soil samples were collected from the first 1 cm of the surface in 27 points along seven topossequences. The material was analyzed by a Vis-NIR-SWIR spectrometer without sample preparation (field conditions) and after drying and sifting. The dry-sifted samples were also analyzed by an X-ray fluorescence equipment to provide the data for the weathering indices calculation. Reflectance data were obtained from sentinel and landsat for the same 27 points. The differences between field-condition and dry-sited samples were analyzed by the subtraction from each other. The data from lab were convoluted to sentinel and landsat bands to compare its shape and its performance on estimating the soil weathering indices with those acquired from satellite data. The differences between the reflectance from samples in field conditions can be very significant for both basaltic and sedimentary parent materials. The surface roughness reduces the reflectance because of the energy dispersion, which reduces the photon return probability. The processed samples showed a higher reflectance on more than 80 % of the points, which can be explained by the roughness reduction and the structure effect on soil surface. However, some cases showed the opposite, with a smaller reflectance to the dry-sifted samples. This fact supports the blocs heterogeneity hypothesis and the clay occlusion. The sample preparation can increase or decrease the reflectance of the soil surface material, depending mainly on roughness, soil structuration and particles occlusion by the structure. The Landsat spectral signatures were more similar to those from convoluted laboratory data than the Sentinel ones. The satellite performance on the estimation of the weathering indices is comparable to those from convoluted laboratory data but is limited by its spectral resolution. Satellites with a higher spectral resolution could achieve higher performance on the estimation of weathering indices. The models for PIA and STi indices were the best ones for both laboratory and satellite data.

Keywords: mixing effect; proximal sensing; remote sensing; XRF; weathering indices

3.1. INTRODUCTION

The use of satellite data on the estimation of soil attributes is wide spread worldwide. However, what is the potential of this data on the estimation of weathering indices? How much is its performance affected by the mixing and by the data resolution? Questions like these drove the present study.

The greatest advantages of using satellite images are the covering power and the data acquisition frequency. The Sentinel and LandSat mission are the most famous and used ones due to the free access and their spatial, spectral and temporal resolutions. The reflectance obtained by both mission has been used on several studies on the soil science (Demattê et al., 2018; Fongaro et al., 2018; Gallo et al., 2018; Gholizadeh et al., 2018; Sayão et al., 2018; Mendes et al., 2019).

However, it is still a question: how good can be a model built with satellite data? The laboratory equipment provides the references to the satellite spectral calibration and can be used under controlled conditions, which allows achieving best models for a given attribute. Thus, the question is: how the resolutions, atmosphere absorption, surface roughness and particle segregation can affect the satellite data and their performance on weathering indices estimation?

To start to solve that question, we proposed this present study. The main hypothesis is that the satellite data can performs like to laboratory convoluted data on the identification of soil surface spectral signatures and for soil weathering indices estimation. Thus, the main objectives on this work were: i) to show the difference of spectral signature between prepared and field conditions samples; ii) to compare the convoluted data from laboratory spectroradiometer with the spectral signatures from Sentinel and Landsat satellites; iii) to build models to predict soil weathering indices with both diffuse reflectance from samples under natural conditions, dry-sifted samples and from satellite images.

3.2. MATERIAL AND METHODS

3.2.1. Study area and data collection

The research was conducted on a 165-ha farm located in Rio das Pedras municipality, SP, Brazil (Figure 1a). The elevation ranges from 543 to 644 m and the parent materials are highly diverse, mainly Basaltic from Serra Geral Formation (KSg) and Sedimentary rocks from Tatuí (Ptt) and Iratí (Pi) formations (Mezzalira, 1989) (Figure 1c). The soil is cultivated with sugarcane and was exposed due to the renewal of planting at the collecting time, which allowed to get satellite images that contain the soils of the area without covering.

Soil samples were collected from the first 1 cm of the surface in 27 points along seven topossequences (Figure 1a and b). The collected material was taken to the laboratory and disposed on Petri dishes with 0.10 m diameter without processing to simulate the field conditions in the laboratory (FL samples). The Vis-NIR-SWIR spectra were registered by a FieldSpec 3 spectroradiometer (Analytical Spectral Devices, ASD, Boulder, CO), which has a

spectral range from 350 to 2,500 nm. The spectral resolution varies for each spectral range, as follows: 1 nm, from 350 to 700 nm; 3 nm, from 700 to 1,400 nm; and 10 nm from 1,400 to 2,500 nm. However, the output data were resampled to 1 nm, resulting in 2,151 channels (Demattê et al., 2019). The optical fiber cable was positioned at 8 cm from the sample surface, which was lit by two halogen lamps (50 W) 35 cm far from the sample platform with a 30º zenith angle. A Spectralon white plate was used to obtain the maximum reflectance reference. The spectral curves comprised an average of three replicates acquired with rotation (90º, 180º and 270º), each with 100 readings to reduce shading and the roughness effects.

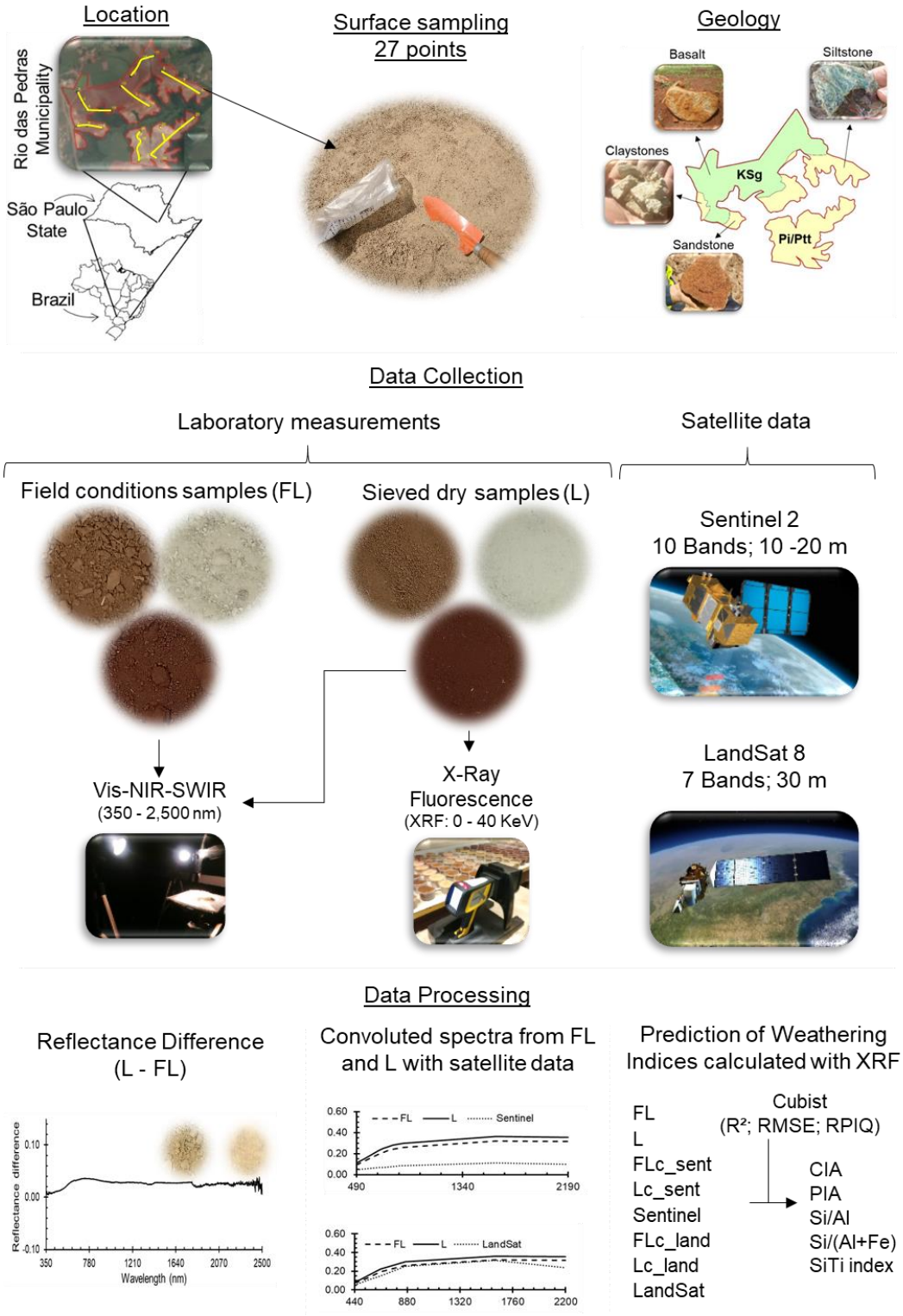

Figure 1. Study flowchart.

After that, the same samples were dried (45 ºC) and sieved (2 mm). The dry-sifted samples were placed on the same Petri dishes and were planed with a spatula to reduce surface roughness (L samples). Subsequently, the same collection procedure described above was performed for the resulting material. A portable X-Ray Fluorescence (pXRF) was used to measure the elemental concentration on the dry-sifted samples. This equipment works with a Silver anode (Ag) X-Ray tube (4 W) in the range from 0 to 40 keV. Calibration was checked by using the NIST 316 alloy, two standard soil samples (SRM 2710a – Montana I Soil; and SRM 2711a – Montana II Soil) and a pure SiO2 sample, both from NIST. It was used two energy beans to optimize the light elements estimation: 0 to 10 keV and 0 to 40 keV. This procedure (0 to 10 keV) improves the signal/noise ratio allowing to get better estimations once high energy scattering increases the noise at low energy channels. The equipment was used on "Soil" mode, which is an internal software that allows estimating the elements concentration in soil-like matrices. The pXRF interacts with matter in an atomic level reporting the chemical composition of the sample for elements with an atomic number above 11. This is a primary method based on direct interactions between X-ray energy and elements, so it can provide a relative elemental concentration of the samples (Weindorf et al., 2012a).

The data obtained from XRF were used to calculate the following soil weathering indices: (Si/Al (Ruxton, 1968); Si/(Al+Fe) (Ruxton, 1968); Chemical Index of Alteration (CIA) (Nesbitt and Young, 1989); Plagioclase Index of Alteration (PIA) (Fedo et al., 1995); and SiTi index (Jayawanderna and Izawa, 1994). It was assumed that the Si and Ca are mobile and the others are immobile during the weathering process. The Si/Al ratio (Ruxton, 1986) informs the loss of silica due to soil evolution process. The Si/Ti index is a ratio between Si and Ti and Al (Jayawanderna and Izawa, 1994). The Chemical Index of Weathering (CIW) (Harnois, 1988) considers the ratio between Al oxide and Ca and Na ones and ranges from 0 to 1. However, the Na content can't be estimated by pXRF and was missed on the indices calculation. In fact, the Na content is frequently very low on the soils studied on this work and is not determined on routine analyses.

Satellite data (reflectance) were extracted from the Sentinel 2 and Landsat 8 missions to each one of the 27 points. The satellite reflectance was obtained from images registered on the same week of the sampling time, to be as closer as possible to the covering conditions. The Sentinel satellite provides three bands in the Vis (Red, green and blue) and one in the NIR (Near Infrared) with a spatial resolution of 10 m. It also has vis-nir-SWIR bands with 20 m pixel sizes. and the Landsat provided 7 bands with 30 meters.

3.2.2. Data analyses

The diffuse reflectance obtained from samples on field conditions and from the dry-sifted ones were analyzed by calculating the difference between them (Figure 1d). This approach was used to show were the differences occurs in each case. Also, these data were convoluted to Sentinel and Landsat simulations. The resulting data were plotted together with the reflectance from satellite images for each point (Figure 1g). The graph representation of the data from the three sources allows identifying visually the points where the spectral signature does not match between them.

The data from FieldSpec (raw and convoluted) and from the satellite were used to build Cubist models to estimate the weathering indices obtained with pXRF. The models were boosted by selecting the best values for "Neighbors" (0, 1, 5 and 9) and "Committees" (1, 10, 50 and 100). All the combinations of these parameters (16) were tested to provide the best one. The best model for each case was utilized to access the following indicators: Coefficient of Determination (R^2); Root Mean Square Error (RMSE); and Ratio of Performance to InterQuartile distance (RPIQ) (Bellon-Maurel et al., 2010). For RPIQ the model quality was classified as follows: RPIQ > 2.00 indicate excellent models; 1.40 < RPIQ < 2.00, reasonable models; and RPIQ < 1.4, unreliable models. These classification was suggested by Chang et al. (2001) for the Residual Prediction Deviation (RPD) and applied to RPIQ (Terra et al., 2015).

3.3. RESULTS AND DISCUSSION

The differences between the reflectance from samples in field conditions can be very significant for both basaltic and sedimentary parent materials (Figure 2). This fact was expected once the sample roughness and the particles organization on the soil structures occurs as a selective process. The particles segregation is a result of the splash and the selective transportation thought the landscape. The fine particles are carred out by the runoff on more sloped landforms while can be deposited on the surface during the water infiltration on more flat soil bodies.

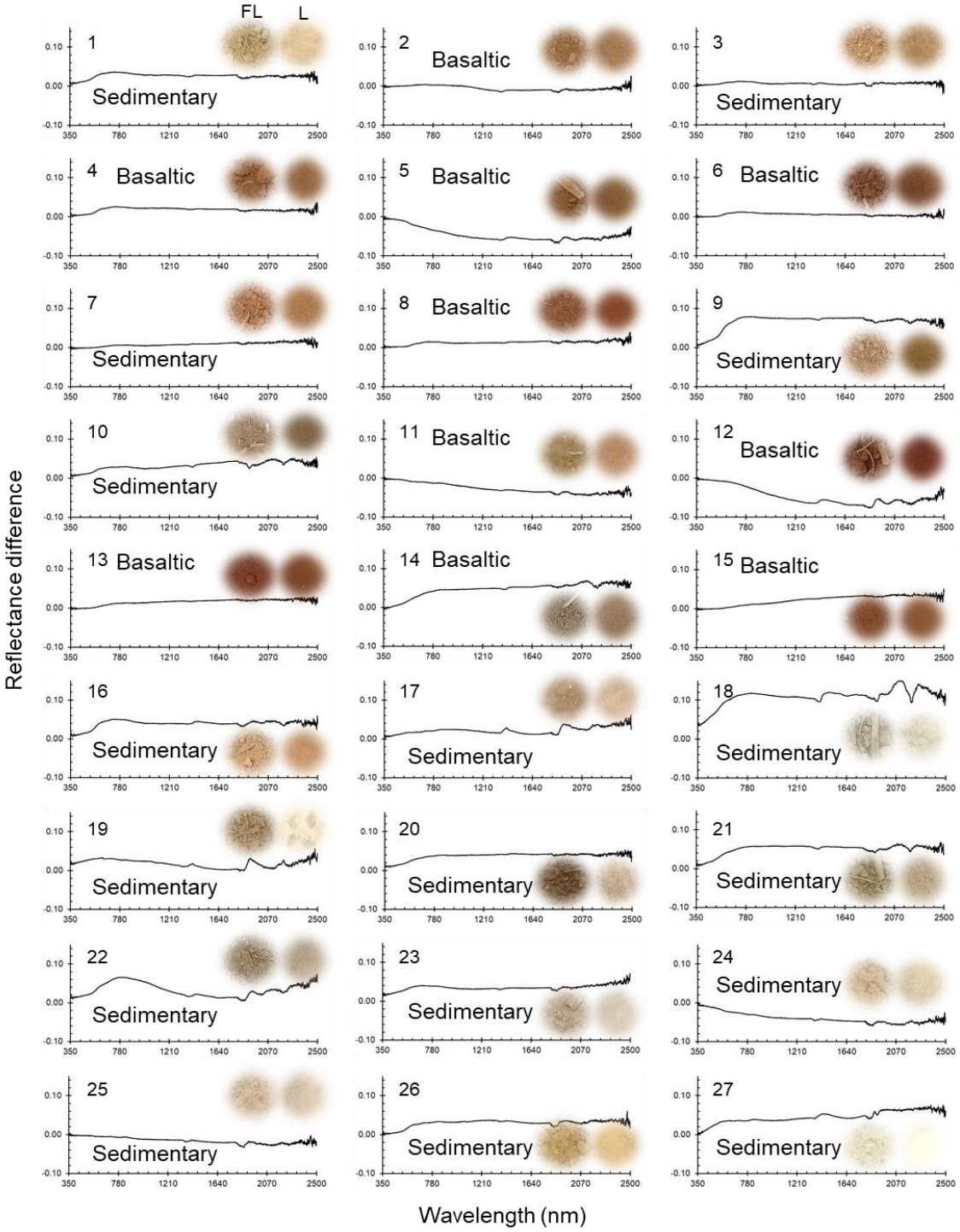

Figure 2. Reflectance difference (350 – 2,500 nm) between field conditions (FL, left) and dry-sifted (L, right) samples collected on the surface of 27 points.

The structure and the size of the blocs formed during the soil development are a function mainly of the clay and Fe contents. Both of these soil components can stabilize the structures formed by the by the organic and inorganic particles on the soil. On the surface this

process is even more evident once the management and weather factor acts strongly than in the undersurface layers. An important fact that occurs during the blocs' formation is the particles occlusion. This process is very important on the soil diffuse reflectance once this property is a result of the electromagnetic radiation with the surface of the sample. It means that if the blocs are not homogeneous, the surface will not represent the real composition of the sample. It is a challenging issue once the soil bodies are naturally strongly altered materials.

The surface roughness reduces the reflectance because of the energy dispersion, which reduces the photon return probability. Large proportion of small structures, or single particles, increase the contact surface of the soil and, consequently, its albedo, while the coarse structures decrease the surface/volume ratio and increase the radiation dispersion pathways (Sarathjith et al., 2014; Gomez et al., 2018). Additionally, the field conditions have remains from plants that have great influence on the diffuse reflectance. However, the cracking of the blocs and the exposure of the occluded particles appears to have a stronger effect on this property.

The processed samples showed a higher reflectance on more than 80 % of the points, which can be explained by the roughness reduction and the structure effect on soil surface. However, some cases showed the opposite, with a smaller reflectance to the dry-sifted samples. This fact supports the blocs heterogeneity hypothesis and the clay occlusion. It is wide spread that the clay absorbs the energy through all the Vis-NIR-SWIR range (Fongaro et al., 2018; Demattê et al., 2018).

The reflectance convoluted to Sentinel bands from 350 – 2,500 nm range showed a very similar behavior (Figure 3) for both samples type (field condition and dry-sifted). However, the spectral curves from Sentinel showed a more pronounced bands on the visible range than the data from the laboratory, which can be associated to the mixing on the pixel. Also, the curves from this mission does not shows a pattern concerning the reflectance intensity. In some cases, it is higher than those from lab and lower in others. Small proportions of green plant debris and straw on the soil surface, or in the mixed soil mass, can manifests, respectively, chlorophyll and carotenoid absorption features in the visible region and higher reflectance intensity in SWIR region (Rodionov et al., 2016).

The Landsat curves are more similar to those obtained in laboratory than those from Sentinel (Figure 4). This fact was not expected once the pixel resolution is smaller than the Sentinel ones. Possibly, the larger pixels caused the average reflectance to be closer of the soil pattern, diluting the effect of green plant debris and straw mixed with the soil mass.

The models built with both laboratory data showed good results for all the weathering indices, except for the CIA and PIA with FL samples. These indices take into account the Ca and K contents, which are on the plant residues. The Ca content probably have the greatest influence once it is on the plant tissue structure.

The results from convoluted spectral signatures were very similar to those from satellite images. In fact, satellite images performed better than laboratory data on all cases, except for Si/Al and Si/(Al+Fe) with Sentinel (Figure 5). These facts support that the satellite data are on its upper limit of the soil reflectance representativeness, been limited the spectral resolution, once it shows a result equals or better than those obtained under controlled conditions and with sample preparation.

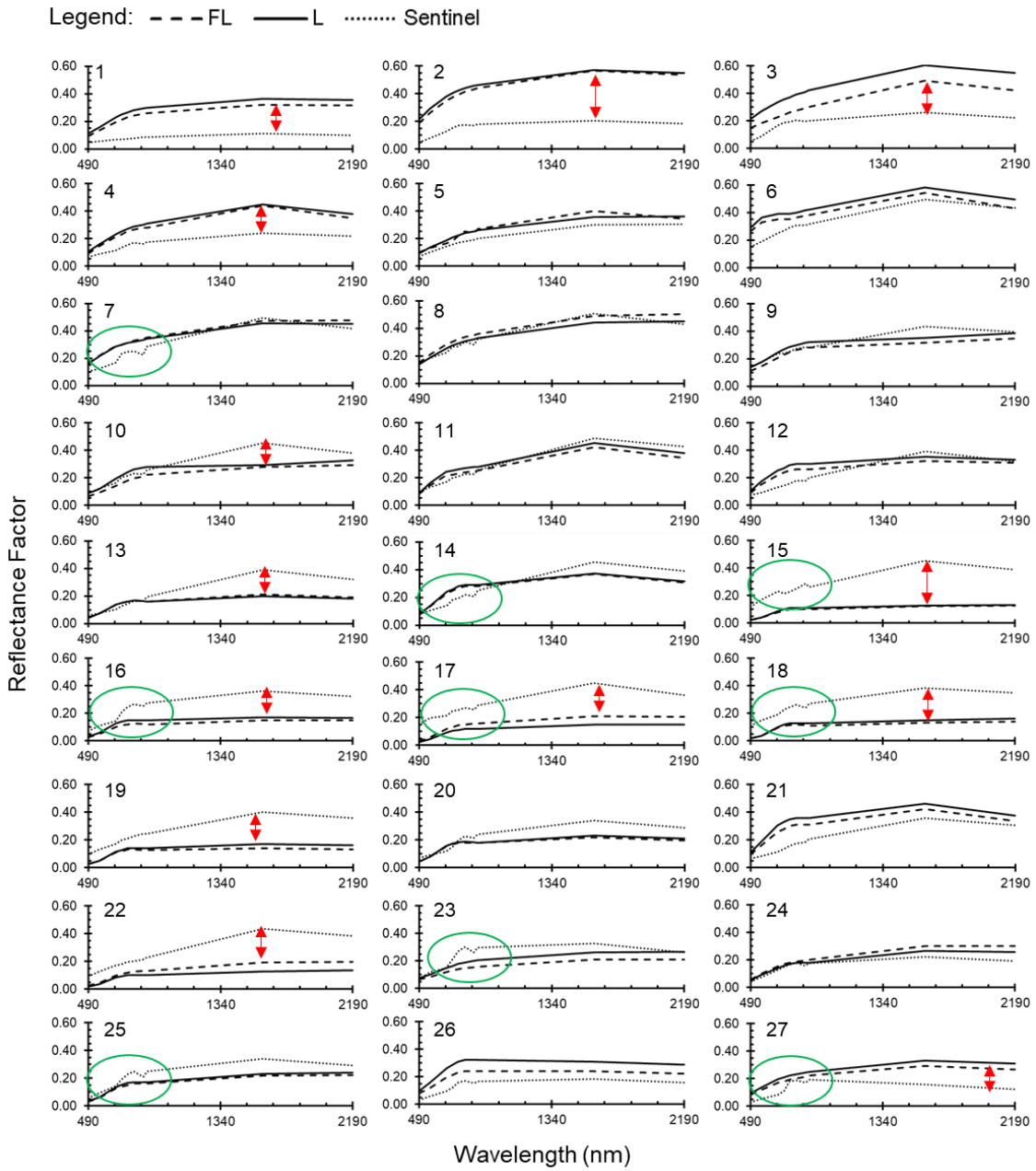

Figure 3. Convoluted spectral signature from field conditions (FL) and dry-sifted (L) surface samples and Sentinel reflectance from 27 points.

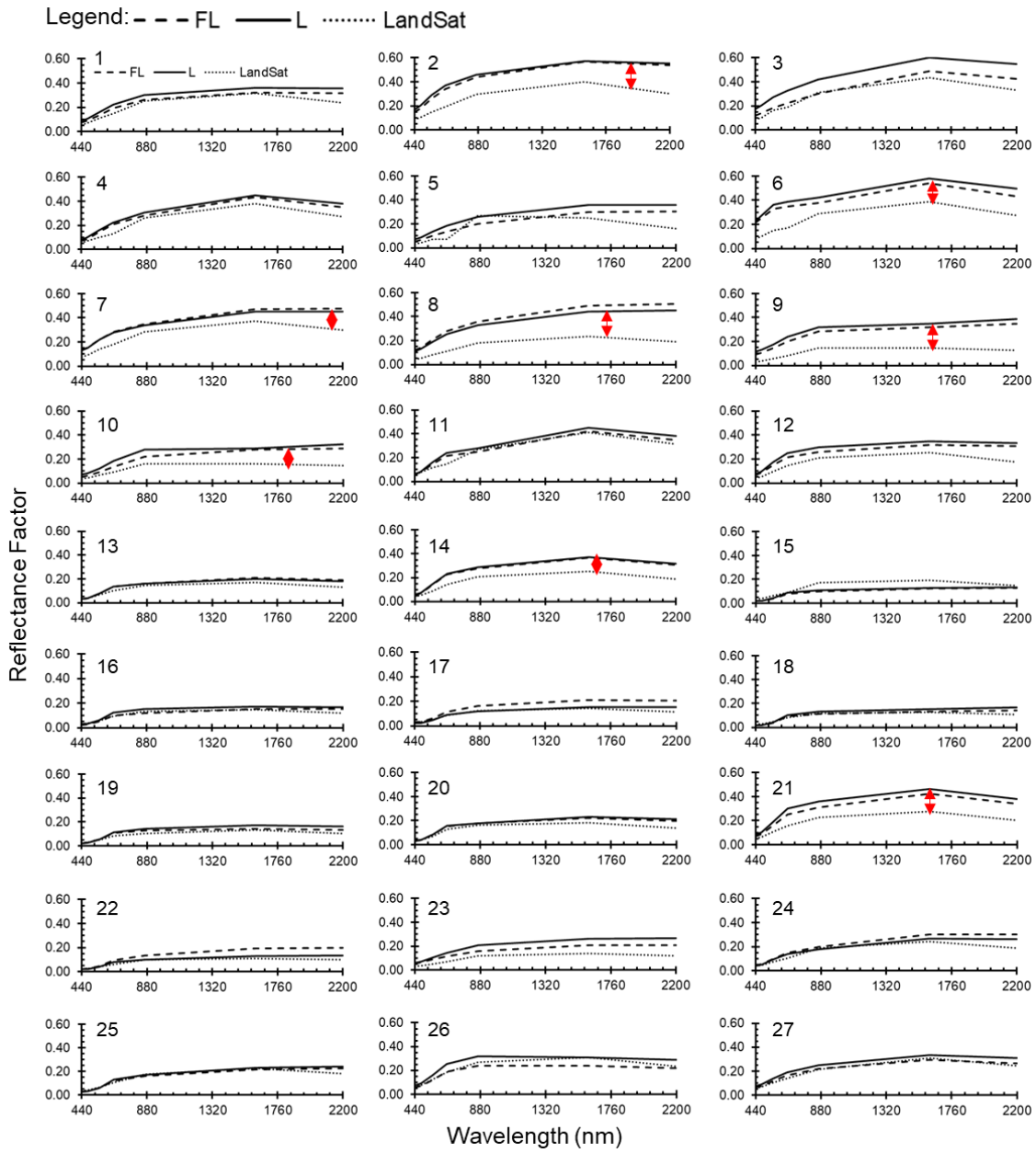

Figure 4. Convoluted spectral signature from field conditions (FL) and dry-sifted (L) surface samples and Landsat reflectance from 27 points.

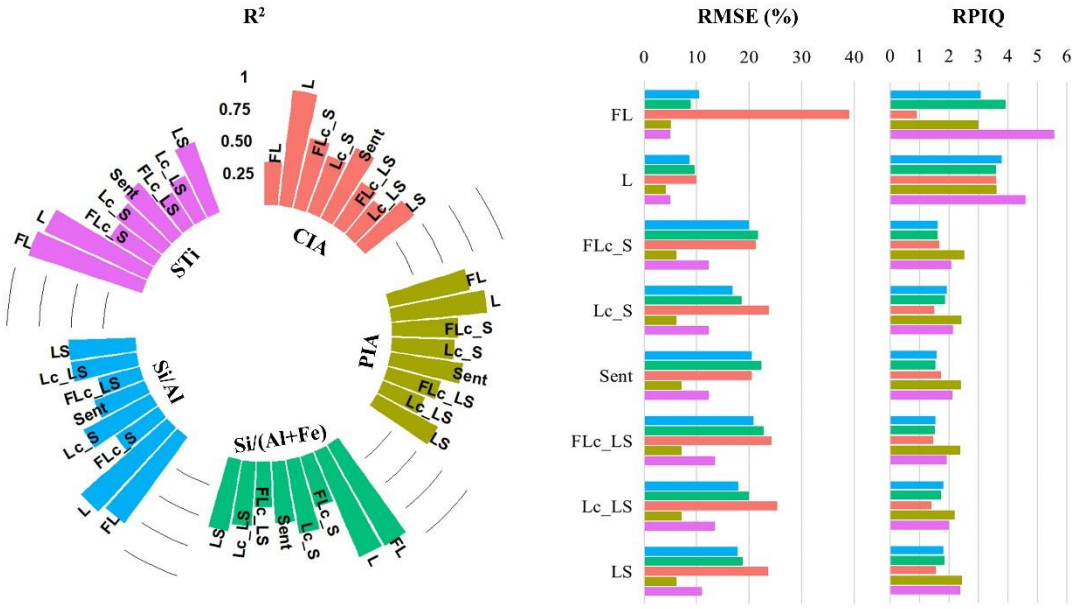

Figure 5. Merit figures from Cubist models with laboratory and satellite data (FL, field conditions in the laboratory; L, laboratory conditions; FLc_S, FL convoluted for Sentinel; Lc_S, L convolved for Sentinel; Sent, Sentinel; FLc_LS, FL convoluted for Landsat; Lc_LS, L convolved for Landsat; and LS, Landsat).

3.4. CONCLUSIONS

a) Sample preparation can increase or decrease the reflectance of the soil surface material, depending mainly on roughness, soil structuration and particles occlusion by the structure.

b) The Landsat spectral signatures were more similar to those from convoluted laboratory data than the Sentinel ones.

c) The satellite performance on the estimation of the weathering indices is comparable to those from convoluted laboratory data but is limited by its spectral resolution.

d) Satellites with a higher spectral resolution could achieve higher performance on the estimation of weathering indices.

e) The models for PIA and STi indices were the best ones for both laboratory and satellite data.

ACKNOWLEDGEMENTS

We are grateful to Geotechnologies in Soil Science Group (GeoCiS/ESALQ-USP; http://esalqgeocis.wixsite.com/english) for team support. We also thank the anonymous reviewers to improve this paper. The MSc scholarship of the first author was provided by the

National Council for Scientific and Technological Development (CNPq). Funding was provided by São Paulo Research Foundation (FAPESP, grant numbers 2014/22262-0, 2016/26124-6, and 2016/01597-9).

REFERENCES

Demattê, J.A.M., Fongaro, C.T., Rizzo, R., Safanelli, J.L., 2018. Geospatial Soil Sensing System (GEOS3): A powerful data mining procedure to retrieve soil spectral reflectance from satellite images. Remote Sens. Environ. 212, 161–175. https://doi.org/10.1016/j.rse.2018.04.047

Fongaro, C.T., Demattê, J.A.M., Rizzo, R., Safanelli, J.L., Mendes, W. de S., Dotto, A.C., Vicente, L.E., Franceschini, M.H.D., Ustin, S.L., 2018. Improvement of clay and sand quantification based on a novel approach with a focus on multispectral satellite images. Remote Sens. 10. https://doi.org/10.3390/rs10101555

Gallo, B.C., Demattê, J.A.M., Rizzo, R., Safanelli, J.L., Mendes, W. de S., Lepsch, I.F., Sato, M. V., Romero, D.J., Lacerda, M.P.C., 2018. Multi-temporal satellite images on topsoil attribute quantification and the relationship with soil classes and geology. Remote Sens. 10. https://doi.org/10.3390/rs10101571

Gholizadeh, A., Žižala, D., Saberioon, M., Borůvka, L., 2018. Soil organic carbon and texture retrieving and mapping using proximal, airborne and Sentinel-2 spectral imaging. Remote Sens. Environ. 218, 89–103. https://doi.org/10.1016/j.rse.2018.09.015

Gomez, C., Adeline, K., Bacha, S., Driessen, B., Gorretta, N., Lagacherie, P., Roger, J.M., Briottet, X., 2018. Sensitivity of clay content prediction to spectral configuration of VNIR/SWIR imaging data, from multispectral to hyperspectral scenarios. Remote Sens. Environ. 204, 18–30. https://doi.org/10.1016/j.rse.2017.10.047

Mendes, W. de S., Medeiros Neto, L.G., Demattê, J.A.M., Gallo, B.C., Rizzo, R., Safanelli, J.L., Fongaro, C.T., 2019. Is it possible to map subsurface soil attributes by satellite spectral transfer models? Geoderma 343, 269–279. https://doi.org/10.1016/j.geoderma.2019.01.025

Rodionov, A., Pätzold, S., Welp, G., Pude, R., Amelung, W., 2016. Proximal field Vis-NIR spectroscopy of soil organic carbon : A solution to clear obstacles related to vegetation and straw cover. Soil Tillage Res. 163, 89–98. https://doi.org/10.1016/j.still.2016.05.008

Sarathjith, M.C., Das, B.S., Vasava, H.B., Mohanty, B., Sahadevan, A.S., Wani, S.P., Sahrawat, K.L., 2014. Diffuse Reflectance Spectroscopic Approach for the Characterization of Soil Aggregate Size Distribution. Soil Sci. Soc. Am. J. 78, 369–376. https://doi.org/10.2136/sssaj2013.08.0377

Sayão, V.M., Demattê, J.A.M., Bedin, L.G., Nanni, M.R., Rizzo, R., 2018. Satellite land surface temperature and reflectance related with soil attributes. Geoderma 325, 125–140. https://doi.org/10.1016/j.geoderma.2018.03.026

4. GEOPHYSICAL SENSORS AND DATA FUSION TO BETTER UNDERSTAND SOIL ENVIRONMENTS

ABSTRACT

The soil environments are highly complex in terms of process and properties. The traditional ways to analyze their attributes and understand its spatial distribution is time consuming and resource intensive. The use of field-based sensors was proposed in this study to assess the spatial variability of soil units without traditional analyzes. The field sensors data were collected in 166 points in a 165 ha area from Rio das Pedras municipality, São Paulo State, Brazil. An Electric Condutivimeter (EM38), a Gamma spectrometer (RS-230) and a Magnetic Susceptibilimeter (KT-10) were used to measure soil properties. The data obtained (i.e., ECa, U, Th, K and MS) were compared to Landsat and Sentinel reflectance images and with to 12 terrain attributes in order to discriminate soil landscape patterns. The study was carried out in two parts: 1st - exploratory and 2nd - mapping. The exploratory analysis consisted of using prediction model (Cubist) to understand the relationships between field sensors and remote sensing data, i.e. from satellite and elevation models. In the second part it was used a "k-means" clustering analysis to cluster the points and the spline method to interpolate its distribution. A Cluster Homogeneity Index (CHI) and a Map Homogeneity Index (MHI) were developed to assess the clustering performance, i.e., the mixing of groups compared to the traditional legacy maps (Soil Classes). The cubist models showed R^2 from 0.04 (Th + Terrain) to 0.97 (Th/K ratio + All data and U/K ratio + All data) and RPIQ from 0.2 (Th/K ratio + LandSat Reflectance) to 4.17 (K content). The models from "All data" were the best ones followed by those from sentinel, except for MS, Th/MS, U/MS and MS/ECa. The Blue band was the most important variable (VIP) from Landsat (B1) and for Sentinel (B490). The CNBL and the Elevation were the most important terrain attributes for all the models. The field sensors attributes are effective on soil environmental mapping. This kind of data allows to better understand the soil bodies and its spatial distribution on the landscape. The data from sensors have a strong relationship with satellite reflectance and terrain attributes. However, it is recommended to develop models with terrain attributes for the same geology. Additionally, as the tacit soil maps quality is limited by the pedologist expertise, sensor informations are useful to identify the transitions between soil bodies directly on the field. With these tools, the professionals can improve the maps quality for many applications. On the other hand, just a few properties can be used to identify soil units, i.e. combining satellite, terrain, ECa and MS were appropriate to map soil derived from basalt, whereas U, Th and K were more efficient for sandstone-derived soils. The use of sensor does not eliminate the need of pedological knowledge for soil mapping. The complete understanding of the full potential is only possible by knowing in depth each sensor and its relationship with the factors and processes on soil formation. Finally, the sample density proved to be the greatest advantage of using field sensors for mapping soils.

Keywords: Field Sensors; Satellite; Clustering; Map Homogeneity Index

4.1. INTRODUCTION

The soil environment is highly complex in terms of processes and properties. The traditional ways to assess its attributes and understand its spatial variability can be arduous due to the high demand of analysis time and financial resources. In soil mapping, denser and

faster data acquisition methods are decisive to understand the full variability of soil conditions and the predominant processes that drives its functions. Thus, field-based geophysical sensors might be an alternative to solve these gaps.

Geophysical sensing provides subsurface information without digging soils. They can reveal important soil properties such as subsurface layers, moisture level, the presence of metallic minerals and trace elements, among others (Romero-Ruiz et al., 2018). From the range of techniques, the Apparent Electrical Conductivity (ECa) is a soil property related to ions, clay and water contents (Brevik and Fenton, 2002; Stadler et al., 2015) that has been correlated to many physico-chemical soil attributes to understand the water flow and distribution of soils on the landscape (Doolittle and Brevik, 2014). This attribute can be measured by electromagnetic induction (EMI), which provides a non-invasive and a fast method to access soil variability at field scale (Heil and Schmidhalter, 2012). The EM38 meter, one of the most used EMI sensors, can take information even from 1.5 m depth (Sudduth et al., 2010). This sensor has been being useful in soil studies once it can provide punctual or continuous measurements in a mobile platform (Doolittle and Brevik, 2014).

Gamma spectroscopy is another useful technique for soil study. The Uranium (U), Thorium (Th) and Potassium (K) are the most active and abundant elements with natural gamma energy emission (Baeza et al., 2016), which can be directly estimated on the field. The distribution of these elements is mainly driven by the parent material, one of the main soil formations factor. The magmatic rocks usually have higher U and Th contents than the sedimentary ones (Guagliardi et al., 2016). However, the distribution on the landscape is also affected by the sediment flow and by the soil bodies concatenation on the landscape.

Another important geophysical method relies on the Magnetic Susceptibility (MS), which is a physical property that measures how much a sample can be magnetized and depends on the soil's constitution (Aydin et al., 2007). In soil science, this property is related to mineralogy and can be helpful in the soil pedons delineation and sediment flux evaluations throughout the landscape (Karchegani et al., 2011).

Similarly, to proximal measurements, the spatial context from remote sensing can support to understand the soil variability. Digital Elevation Models from SRTM and the reflectance from satellite images (Landsat and Sentinel-2) are the main free available data that can be used on landscape analysis. Orbital data are commonly used to estimate surface soil attributes based on its reflectance (Sayão et al., 2018; Mendes et al., 2019; Salazar et al., 2020). Terrain attributes are also frequently associated to digital soil mapping (Yang et al., 2020; Zijl et al., 2019). One of the main contributions coming from these data (satellite and terrain) is the information continuity throughout the surface, which enables a better representation of the landscape. In fact, traditional soil mapping is based more based on surface observations than opening a vast number of soil profiles, which are more appropriate

to identify and validate the identified landscape units using a few and selected quantity of trenchs.

In this context, we proposed to study the relationship between field sensors, terrain attributes, and satellite surface reflectance and how well geophysical sensors alone and together with terrain and satellite data can identify variations among soil bodies with the following main objectives: i) Find the relationship between geophysical sensors and satellite and terrain attributes by using the Cubist models; ii) Study the correspondence between sensor-based maps and the tacit one at farm scale (1:10.000) by using the Map Homogeneity Index developed in this work; iii) Discuss the best match map based on soil landscape processes: what conditions define each soil class? Is the proposed approach effective on soil bodies differentiation?

4.2. MATERIAL AND METHODS

The research was conducted in a 165-ha farm located in Rio das Pedras municipality, SP, Brazil (Figure 1a). The elevation varies from 543 to 644 m and the parent materials are highly diverse, where the soils are mainly formed from Basaltic rocks of Serra Geral Formation (KSg) and Sedimentary rocks from Tatuí (Ptt) and Iratí (Pi) formations (Mezzalira, 1989). The soil is cultivated with sugar-cane and was exposed during the field campaign due to renewal of crops, which allowed to get satellite images containing only bare soils without any other land cover.

The data were collected in 166 points using geophysical field sensors to measure the following attributes: Apparent Electrical Conductivity (ECa); U, Th and K; and the Magnetic Susceptibility (MS) (Figure). On-the-go sensors has their main advantages on given information directly in field, what allows to improve the data collection quality and its representativeness. The ECa was measured with an EM38 equipment which induces an electric current on the soil. This current in turn produces a secondary magnetic field which is captured by the sensor (Brogi et al., 2019). The U-ppm, Th-ppm and K-% where estimated by a Handheld Gamma-Ray Spectrometer (RS-230). This equipment has a 103 cm^3 Bismuth Germanate Oxide detector and works from 30 to 3,000 keV. The MS was assessed with a KT-10, that measures the susceptibility that a given sample has to be magnetized by induction. The “zero” susceptibility was registered in the air.

The statistical analyses were carried out in two parts (Figure 1a, b). The first one was numerical, by using the CUBIST method (Quinlan, 1992) to show the relationship among data from sensors and that from satellite images and terrain attributes. Models for each sensor data (i. e., Attribute or Ratio) were constructed with LandSat (6 bands) and Sentinel reflectance (10 bands) and Terrains attributes (12) (Figure 2). The terrain attributes used were:

Elevation (Elev); Slope; Aspect; Convergence Index (CI); Topographic Wetness Index (TWI); Total Catchment Area (TCA); LS Factor (LS); Channel Network Base Level (CNBL); Channel Network Density (CND); Valley Depth (VD); Relative Slope Position (RSP); and Topographic Position Index (TPI). All of these data were sampled to the same 166 geophysical collecting points. This approach homogenizes the spatial data resolution from the data sources.

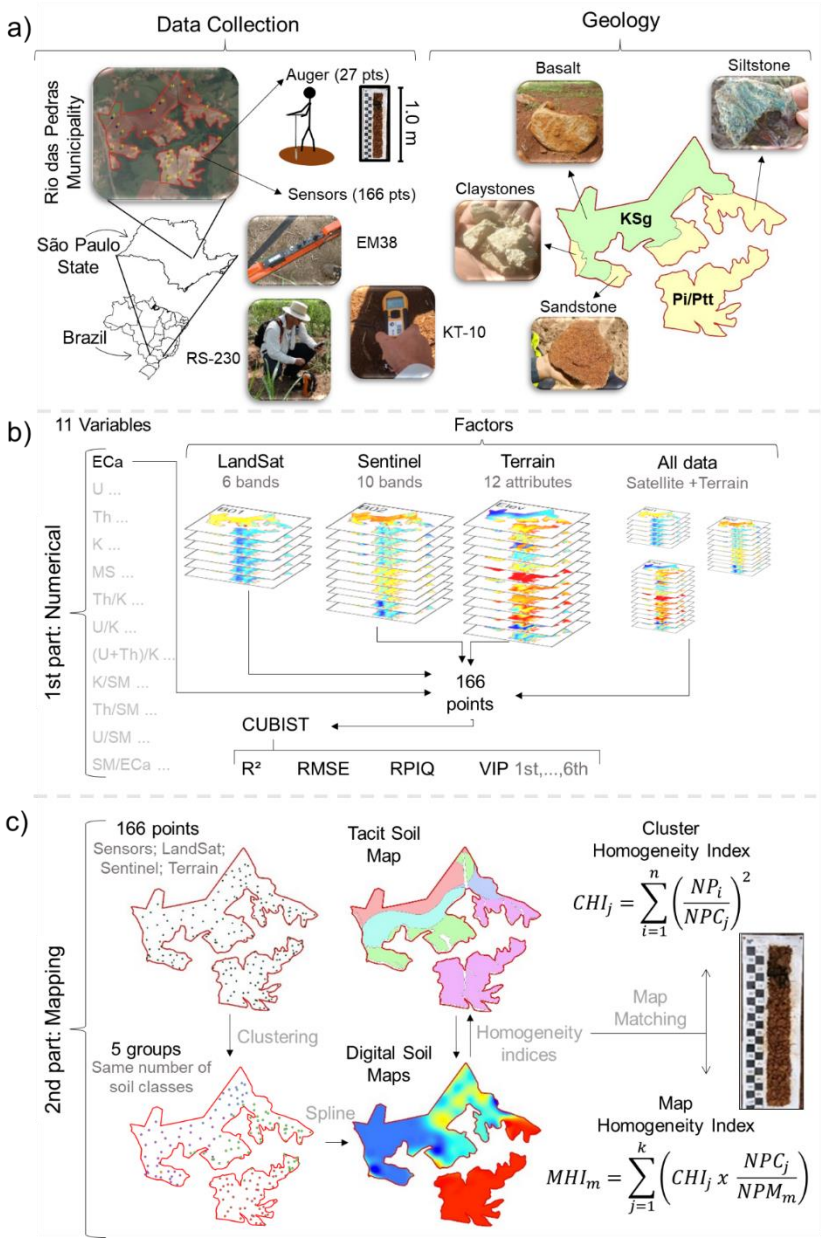

Figure 1. Study area characterization, data collection and analysis.

The CUBIST method was used to show the relationships among geophysical and remote sensing data (Figure 1b). The models were boosted by selecting the best values for "Neighbors" (0, 1, 5 and 9) and "Committees" (1, 10, 50 and 100). All the combinations of

this parameters (16) were tested to provide the best one. The best model for each case was utilized to access the following indicators: Coefficient of Determination (R^2); Root Mean Square Error (RMSE); and Ratio of Performance to InterQuartile distance (RPIQ) (Bellon-Maurel et al., 2010); and the first six most important variables (Variable Importance: VIP). For RPIQ the model quality was classified as follows: RPIQ > 2.00 indicate excellent models; 1.40 < RPIQ < 2.00 indicate reasonable models; and RPIQ < 1.4, unreliable models. These classification was suggested by Chang et al. (2001) for the Residual Prediction Deviation (RPD) and applied to RPIQ (Terra et al., 2015).

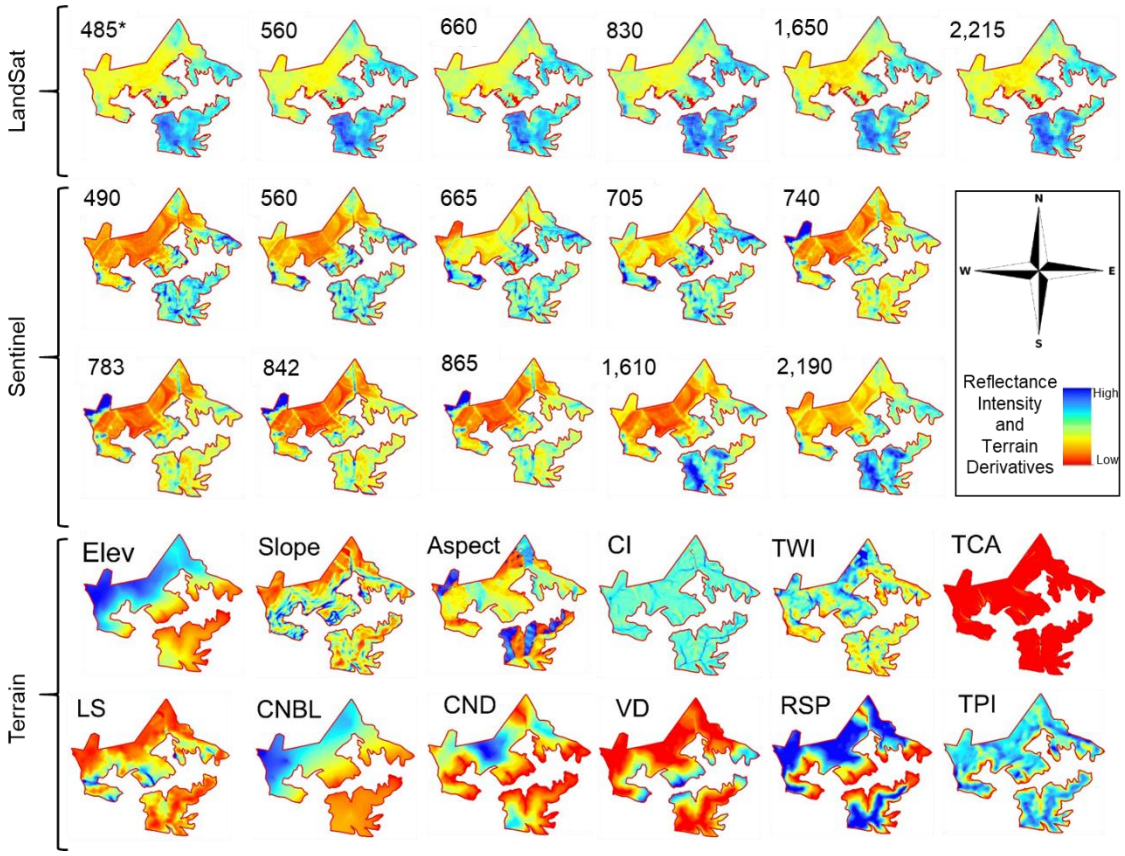

Figure 2. Satellite and terrain predictors used on modelling and mapping the soil environments. *Band Center Wavelength (nm); Elevation (Elev); Slope; Aspect; Convergence Index (CI); Topographic Wetness Index (TWI); Total Catchment Area (TCA); LS Factor (LS); Channel Network Base Level (CNBL); Channel Network Density (CND); Valley Depth (VD); Relative Slope Position (RSP); Topographic Position Index (TPI).

The second part was to generate surfaces by using “K-means” clustering and Spline (Franke, 1982) approaches (Figure 1c). Each field data and ratio were used on grouping alone and with LandSat Reflectance, and with Sentinel reflectance, and with Terrain attributes, and with all data together (Figure 1c). The number of clusters was the same as the number of soil classes in the tacit map (i.e., five). The number of clusters was fixed to allow the comparison

between maps and shows the matching between the sensor-based soil map and the traditional one.

A Cluster Homogeneity Index (CHI) and a Map Homogeneity Index (MHI) were developed (Equations 1 and 2) to access the grouping quality, i.e., the mixing of groups from the Tacit soil map on each cluster and for the whole map. The Homogeneity indices vary from 0 to 1. A cluster with only one group from the base map will have "1" as homogeneity score (HS). However, a group with half of its points in a group and half in another one will have "0.5" as HS. The HS tend to zero when a given cluster has many groups from reference map without presenting predominant ones. The MHI is based on the clusters homogeneity (Equation 2). A map with clusters completely matching the reference one will have the highest homogeneity score. These indices were calculated for every sensor-based map (e.g., 60) to identify which one best matches the traditional one.

Equation 1: Cluster Homogeneity Index (CHI).

$$CHI_j = \sum_{i=1}^{n} \left(\frac{NP_i}{NPC_j} \right)^2$$

Where:

n: Nº of classes *i* in cluster *j*.

NP_i: Nº of points in class i.

NPC_j: Nº of points in cluster *j*.

Equation 2: Map Homogeneity Index (MHI).

$$MHI_m = \sum_{j=1}^{k} \left(CHI_j \; x \; \frac{NPC_j}{NPM_m} \right)$$

Where:

k: Nº of clusters on map m.

CHIj: Homogeneity Index for Cluster j.

NPCj: Nº of Points in Cluster j.

NPMm: Nº of Points on map

4.3. RESULTS AND DISCUSSION

4.3.1. Exploratory analysis

4.3.1.1. Models Accuracy

The cubist models showed R^2 from 0.04 (Th + Terrain) to 0.97 (Th/K + All data and U/K + All data) and RPIQ from 0.2 (Th/K + Landsat Reflectance) to 4.17 (K) (Table 1). The models from "All data" were the best ones followed by those from sentinel, except for MS, Th/MS, U/MS and MS/ECa. For MS and MS/ECa the models with Landsat data were better than those from Sentinel, and for Th/MS and U/MS, Sentinel data provides the best ones. The ratios between attributes improved the R^2, but reduced the RPIQs.

In fact, among 48 models, only six were accurate in both R^2 and RPIQ and only for U, K, MS and for the ratio between K/MS (Table 1). Sentinel data is present on all models. This fact is strongly related to the contrasting geology observed in the area, once it drives the

soil color and clay content. This attributes can be well estimated by using Landsat data, however, Sentinel images have higher spatial resolution and higher number of bands, which can provide more accurate estimates due to the lower mixing on the reflectance and to the bands.

The models with Terrain derivatives showed low accuracy for all sensors attributes. However, MS, Th/K and U+Th/K models (with terrain data) showed a high R^2, suggesting that this attributes can be driven by the landform. In fact, the MS and K are highly affected by the water flow and the U and Th contents are highly affected by the particles flow on de landscape. On the other hand, the studied area have a complex combination of geology and landforms. The same shape occurs in different geology. This fact reduces the capability of the model to explain the relationship between sensors data and terrain derivatives.

4.3.1.2. Variable Importance

The complexity of environments (i.e., geology and terrain) led to different patterns for each geophysical attribute. This fact has great influence on the models behavior and its representativeness because each one of the events may have their own model. However, it is possible to identify the most important variables (MIV) working on the models (Table 1). The bands from the blue range were the MIV from both Landsat (B1) and Sentinel (B490) data followed by the Red ones and by the Infrared bands (Table 1). This fact happened due to the relationship between soil color and its attributes, as mineralogy, and clay and organic carbon content. In fact, the data from field sensors are also strongly driven by these soil attributes. Mendes et al. (2019) estimated subsurface attributes using the relationship between surface reflectance from LandSat 5 and the spectral behavior of the soil. These authors reached that this relationship allows to model subsurface attributes.

The CNBL and the Elevation were the MIV among terrain attributes for all the models (Table 1). Both of these attributes are related to the geologic vertical organization once it has a well-defined sequence on the landscape. The biggest challenge on using terrain derivatives on soil modeling are the similarities between shapes from different geologic materials. In fact, this issue can confuse the models once it will have the same terrain attribute for completely different soil bodies. Thus, it is recommended to build models separately or consider the geology as one of the factors.

Table 1. Cubist models quality parameters from field sensors data associated to satellite reflectance and terrain attributes.

Attribute	Data	R^2	RMSE	RPIQ	Variable Importance					
					1º	2º	3º	4º	5º	6º
ECa	LandSat	0.45	30.52	1.15	B1	B2	B3	B4	B6	-
	Sentinel	0.55	28.02	1.26	B490	B2190	B740	B865	B560	B783
	Terrain	0.36	32.87	1.07	CNBL	Aspect	TWI	CI	Elev.	CND
	All data	0.66	24.66	*1.43	B1	Elev.	Slope	Aspect	LS	RSP
U	LandSat	0.45	1.04	*1.99	B1	B5	B6	B4	-	-
	Sentinel	0.56	0.95	**2.19	B490	B560	B842	B705	B740	B783
	Terrain	0.31	1.17	*1.77	CNBL	Elev.	VD	CND	Slope	Aspect
	All data	*0.76	0.72	**2.87	B1	B665	CNBL	Elev.	B560	B2190
Th	LandSat	0.39	3.66	1.39	B3	B4	B5	B6	-	-
	Sentinel	0.56	3.14	*1.61	B865	-	-	-	-	-
	Terrain	0.04	4.58	1.11	Elev.	-	-	-	-	-
	All data	0.65	2.85	*1.78	Elev.	-	-	-	-	-
K	LandSat	0.63	0.33	**2.70	B4	B1	B2	B3	B5	B6
	Sentinel	*0.77	0.27	**3.38	B490	B865	B2190	B740	B783	B1610
	Terrain	0.53	0.38	**2.36	CNBL	Elev.	CND	LS	RSP	Aspect
	All data	**0.85	0.21	**4.17	CNBL	B490	B1	TCA	RSP	B783
MS	LandSat	**0.89	6.96	*1.54	B1	B2	B4	B6	B3	B5
	Sentinel	**0.87	7.68	1.39	B490	B2190	B1610	B865	B842	B740
	Terrain	*0.78	9.72	1.10	CNBL	Elev.	TPI	CI	LS	TCA
	All data	**0.94	5.43	*1.97	B1	B2	Elev.	B6	B1610	CNBL
Th/K	LandSat	0.62	231.54	0.20	B1	B2	B4	B3	B5	B6
	Sentinel	**0.92	103.46	0.45	B490	B865	B2190	B842	B740	B560
	Terrain	**0.90	146.07	0.32	Elev.	LS	VD	TPI	CI	CND
	All data	**0.97	75.42	0.61	Elev.	B490	LS	B4	VD	TPI
U/K	LandSat	0.63	91.59	0.18	B1	B4	B3	B2	B6	B5
	Sentinel	**0.88	51.31	0.32	B490	B865	B2190	B740	B560	B783
	Terrain	0.23	129.04	0.13	Elev.	LS	CNBL	TWI	RSP	Slope
	All data	**0.97	30.67	0.54	Elev.	VD	LS	B490	B865	TPI
(U+Th)/K	LandSat	*0.79	230.14	0.26	B1	B5	B3	B2	B4	B6
	Sentinel	**0.93	133.12	0.45	B490	B865	B740	B783	B560	B2190
	Terrain	**0.92	144.59	0.42	Elev.	LS	CND	TPI	TWI	VD
	All data	**0.94	118.42	0.51	Elev.	LS	B560	B490	B2190	CND
K/MS	LandSat	0.47	1.27	1.18	B2	B1	B3	B5	B4	B6
	Sentinel	**0.83	0.75	**2.01	B865	B490	B560	B665	B705	B1610
	Terrain	0.46	1.28	1.17	CNBL	Aspect	RSP	Elev.	CND	Slope
	All data	**0.91	0.52	**2.89	CNBL	B490	B6	B842	B705	Elev.
Th/MS	LandSat	0.40	16.32	1.04	B1	B3	B4	B5	-	-
	Sentinel	*0.74	12.25	1.39	B490	B560	B665	B783	B865	B1610
	Terrain	0.45	15.58	1.09	CNBL	CND	Elev.	VD	RSP	TWI
	All data	0.64	13.28	1.28	Elev.	B490	CNBL	VD	CND	B665
U/MS	LandSat	0.26	5.88	0.82	B1	B3	B4	B5	-	-
	Sentinel	*0.79	4.08	1.17	B490	B665	B1610	B2190	-	-
	Terrain	0.43	5.19	0.93	Elev.	CNBL	CND	-	-	-
	All data	0.60	4.45	1.08	Elev.	B490	LS	B1	CNBL	CND
MS/ECa	LandSat	*0.72	0.32	0.31	B1	B4	B5	B6	B2	-
	Sentinel	0.61	0.37	0.27	B490	B842	B560	B783	B865	B1610
	Terrain	0.45	0.44	0.23	CNBL	TPI	CND	CI	VD	-
	All data	**0.85	0.24	0.41	B490	B1	B842	B705	B560	CNBL

R^2: * for $0.7 < R^2 < 0.8$; ** for $R^2 \geq 0.8$; RPIQ: * for $1.4 < RPIQ < 2.0$; ** for $RPIQ \geq 2.0$. ECa: Apparent Electrical Conductivity; U: Uranium; Th: Thorium; K: potassium; Magnectic Susceptibility; Bi: Band I; Elevation (Elev); Slope; Aspect; Convergence Index (CI); Topographic Wetness Index (TWI); Total Catchment Area (TCA); LS Factor (LS); Channel Network Base Level (CNBL); Channel Network Density (CND); Valley Depth (VD); Relative Slope Position (RSP); Topographic Position Index (TPI).

4.3.2. Mapping

4.3.2.1. Map Homogeneity Index (MHI)

The MHI were developed here aiming to understand and quantify the correspondence between soil maps built based on geophysical data and the one derived from traditional method (Tacit Soil Maps). Nevertheless, this index can be used to compare maps from other sources. In the present case, the sensor-based soil maps showed MHI's from 0.38 to 0.71 (Figure 3) and good agreement with geological contrasts. The greater level of detail shown on sensor-based maps is noticeable at the expense of the traditional survey. This fact could give support to the development of more detailed soil maps.

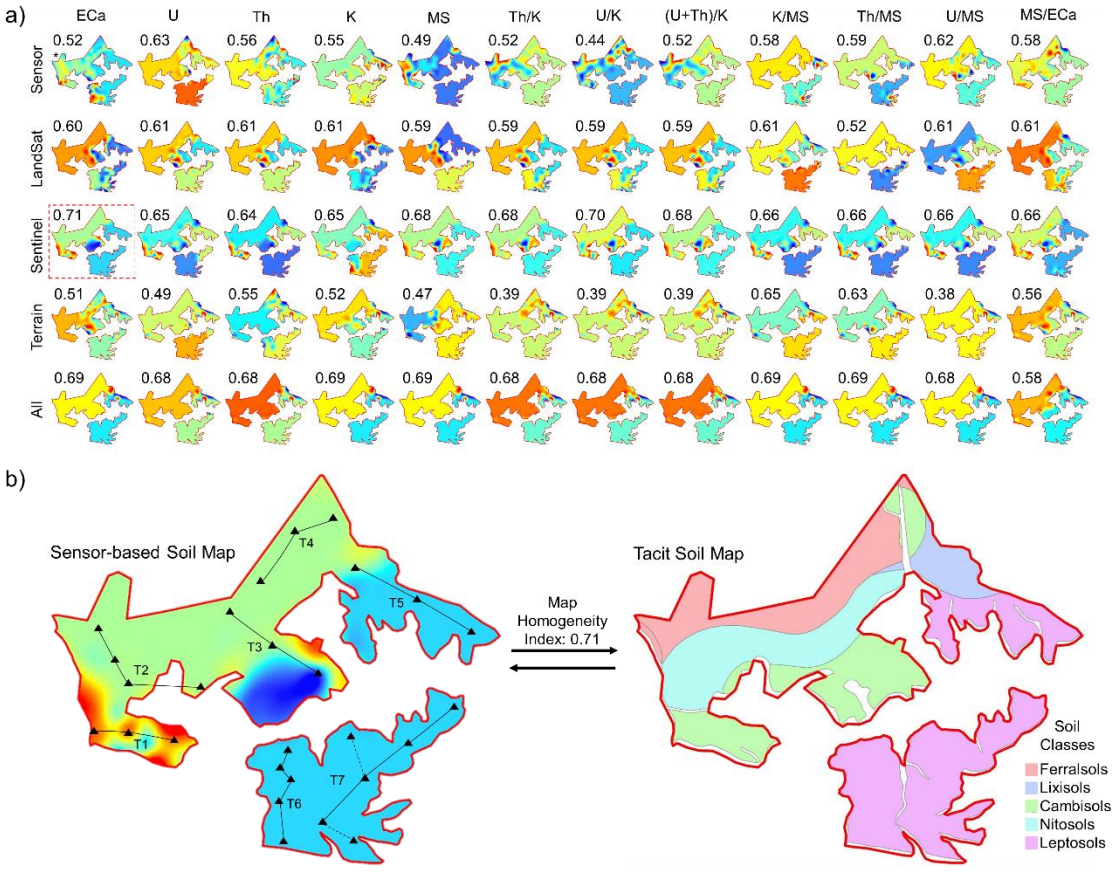

Figure 3. a) Spline from grouping analyses for each combination of geophysical sensor data and satellite and terrain attributes with respective Map Homogeneity Indices (MHI). b) Tacit soil map, sensor-based soil map with the best MHI and topossequences for soil profiles investigations.

The field sensors denoted different patterns through the area, showing that they can provide complementary information to the mapping process (Figure 3a). Among the field sensors maps, the best MHI's were found for U content (0.63) and for U/MS ratio (0.62) and the worst was achieved for U/K (0.44) (Figure 3a). U, Th, K, K/MS, Th/MS and U/MS did

not differentiate the Ferralsols, Nitosols and Cambisols from the west part (T1 and T2). However, it seems that these data can find differences among sedimentary sources. The opposite could be observed for ECa and MS, which was better on shows segmentations where the basaltic material predominates. Alomari et al. (2019) found strong difference by studying contrasting soils and geological formations. The unconsolidated material showed the lowest gamma radiation.

Among all the maps (Figure 3a) only the ones based on MS, Th/K, U/K and (U+Th)/K could express the differences between Ferrasols and Nitosols. The differentiation between these soil bodies is a challenge for digital soil mapping once their clay content and structure are very similar when developed from de same parent material. However, the Nitosols have a greater amount of magnetic minerals than Ferralsols due to its lower weathering rate and to the mixing that occurs during the Ferralsols formation. Those ratios express the accumulation of U and Th at the expense of the K content, which in fact can differentiate these two types of soil, once the Nitosols have a higher elements content than Ferralsols.

The maps built using satellite images did not find differences between Ferralsols and Nitosols (Figure 3a). This fact is due to the similarity concerning the surface color between these soil units. In fact, the surface reflectance can be saturated and does not shows slights differences between these soil classes. Although some sensors were able to distinguish these soils, it is only one data while satellite have six (LandSat) or ten (Sentinel) variables. This fact leads to the superposition of the sensors data and consequently to the loss of its details.

The best match (MHI = 0.71) was provided by the combination of ECa and Sentinel data (Figure 3b). This map shows a more detailed description in the topossequences 1 (T1) and in the end of the T3. These results are corroborated by the simulated profiles (Figure 4). However, the soils are not well differentiated in T4 and T2. This fact is due to the similarities in the colors along these topossequences, as discussed above. However, the soil profiles from T4 have strong differences between them, showing red, gray and yellow matrices (Figure 4). Nevertheless, the surface layers from all of them are dark, which may have led to the error. In fact, this topossequences have been developed in the same parent material (Figure 1) but in distinct landforms (Figure 2), which leads to differences in water dynamics and losses of solutes, mainly Iron. The water flow determines the solubilization and the translocation through the soil profile. The profiles in the T4 are in distinct relative positions on the landscape. The higher position makes the profile 12 remain red because of the better drainage while the 11 one has lost some iron, becoming yellow. The profile 14 shows the strongest loss of iron, which lead it to be gray. This profile is not in the lowest position considering the whole area, but it is a concentration area (Figure 2, TWI, CND, RSP), which increased the water residence time and the iron solubilization.

The maps built with terrain attributes had the worst match with the traditional one. The terrain derivatives combinations with Th/K, U/K, (U+Th)/K and U/MS were not even able to differentiate the geological materials (Figures 1 and 3a) reaching the lowest MHIs among all maps. This fact was not expected since the U, Th and K contents reached better results when used alone (Figure 3a). It can be associated to the changing of patterns due to the ratio calculation and to the already discussed terrain confounding behavior. In fact, the terrain data (12 variables) superposed the field sensors one (one variable).

Any one of the combinations with terrain derivatives were able to distinguish Ferralsols from Nitosols despite of their well-known differences concerning slope and position on the landscape. Although the landform is an important factor that drives the differentiation in this case, terrain derivatives were also not able to distinguish Ferralsols from Nitosols.

The tacit map depends on the knowledge that are not easy to traduce in practical and not subjective soil mapping technics. Thus, the sensors can provide good information with high density which allows to investigate the soil bodies looking for several applications. In fact, multiple applications maps are more economically viable, once it adds value to the land and directs it to the most appropriate use. However, the sensors-base soil maps still need to be studied because of its complexity and of the multicollinearity among sensors data.

4.3.2.2. Simulated Profiles

The simulated soil profiles from T6 and T7 shows strong differences between the soil bodies (Figure 4). However, neither sensor-based soil map nor the tacit one were able to show it. In fact, some variation on this area (T6 and T7) can be seen on the ECa, Th, K, ECa + LandSat, Th/K + LandSat, U/K, (U+Th)/K + LandSat, MS/ECa + LandSat, K + Sentinel and on the Th + Terrain maps. The soil bodies in this part of the area were developed above sedimentary rocks which have a high level of complexity once it depends on the energy and the sources of material on the cycles of sedimentation.

The T5 was well represented in all the maps, excep in Th/MS + LandSat and MS + LandSat. This toposequence changes from basaltic material to the sedimentary one, which leads to a high contrast between the soil bodies (Figure 4). In fact, the elevation goes from 604 to 555 m in 720 m and different materials are exposed to surface processes.

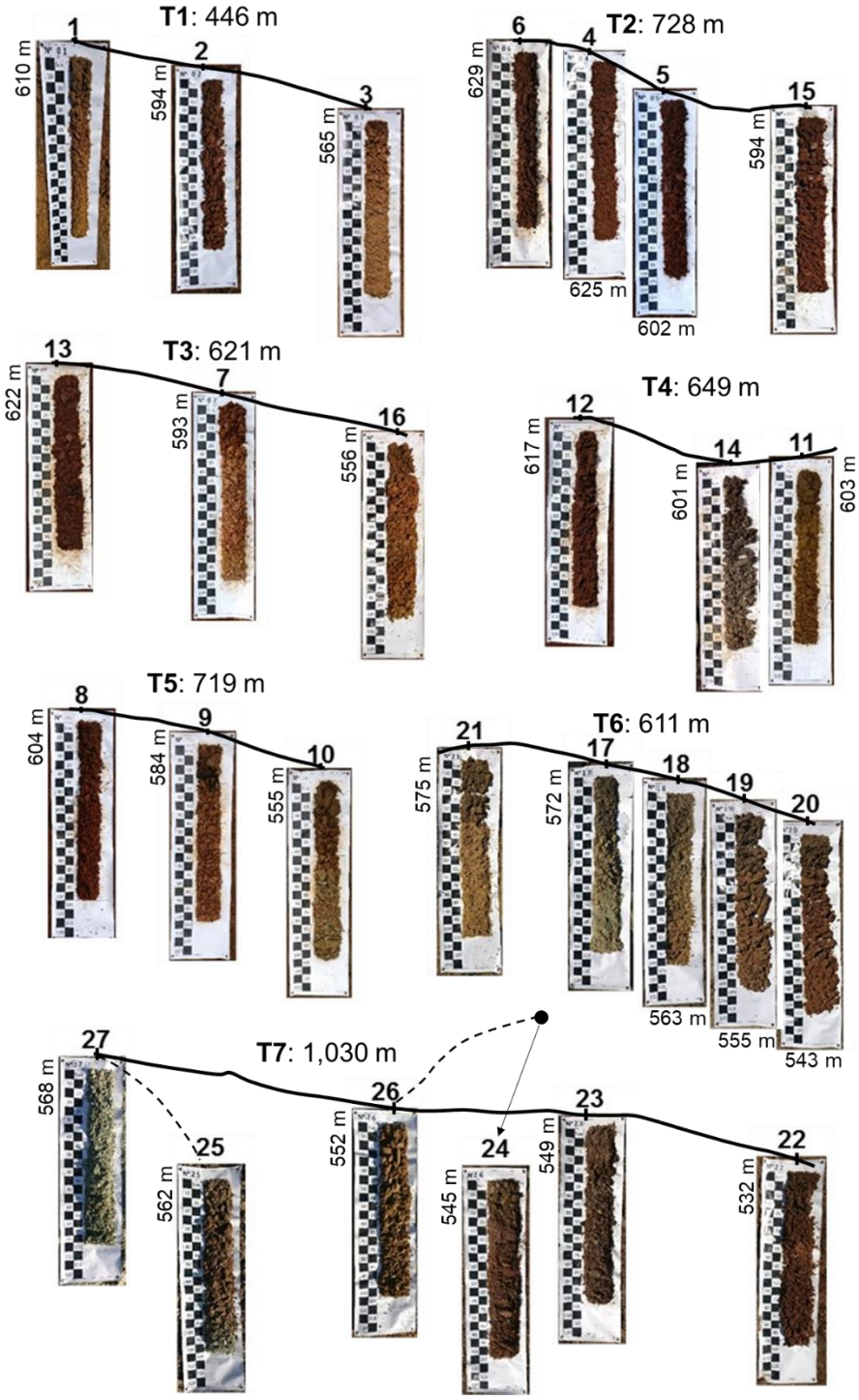

Figure 4. Simulated soil profiles and their positions in topossequences.

4.4. CONCLUSIONS

a. The field sensors attributes are effective on soil units mapping. This source of data allows to better understand the soil properties and its spatial distribution on the landscape.

b. The data from field-based sensors have a strong relationship with satellite reflectance and terrain attributes. However, it is recommended to develop models with terrain attributes for the same geology.

c. The legacy soil maps quality is limited by the surveyor. The sensors are useful to identify the transitions between soil bodies directly on the field. With these tools, the professionals can improve the maps quality for many applications.

d. Its recommended to combine a few multiple sources of data instead of all the available options.

e. ECa e MS are better to identify transitions between basaltic soils, while U, Th and K are more appropriate for soils derived from sandstones.

f. The use of sensors does not eliminate the need for pedological knowledge for soil mapping. The complete understanding of the generated figures is only possible by knowing in depth each sensor and its relationship with the factors and processes of soil formation. The sample density is the great advantage of using field sensors for the work of the pedologist.

ACKNOWLEDGEMENTS

We are grateful to Geotechnologies in Soil Science Group (GeoCiS/ESALQ-USP; http://esalqgeocis.wixsite.com/english) for team support. We also thank the anonymous reviewers to improve this paper. The MSc scholarship of the first author was provided by the National Council for Scientific and Technological Development (CNPq). Funding was provided by São Paulo Research Foundation (FAPESP, grant numbers 2014/22262-0, 2016/26124-6, and 2016/01597-9).

REFERENCES

Alomari, A. H., Saleh, M. A., Hashim, S., Alsayaheen, A., Investigation of natural gamma radiation dose rate (GDR) levels and its relationship with soil type and underlying geological formations in Jordan, Journal of African Earth Sciences, Volume 155, 2019, Pages 32-42, ISSN 1464-343X, https://doi.org/10.1016/j.jafrearsci.2019.04.006.

Aydin, A., Ferré, E. C., Aslan, Z., The magnetic susceptibility of granitic rocks as a proxy for geochemical composition: Example from the Saruhan granitoids, NE Turkey, Tectonophysics 441 (2007) 85–95, doi:10.1016/j.tecto.2007.04.009.

Baeza, J.A., Corbacho, J., Guillén, Accuracy associated with the activity determination by in situ gamma spectrometry of naturally occurring radionuclides in soils, Journal of Environmental Radioactivity, Volumes 162–163, 2016, Pages 219-224, ISSN 0265-931X, https://doi.org/10.1016/j.jenvrad.2016.05.024.

Bellon-Maurel, V., Fernandez-Ahumada, E., Palagos, B., Roger, J-M, McBratney, A. Critical review of chemometric indicators commonly used for assessing the quality of the prediction of soil attributes by NIR spectroscopy. Trac-Trend Anal Chem. 2010;29:1073-81. https://doi.org/10.1016/j.trac.2010.05.006

Brevik, E.C., Fenton, T.E., 2002. The relative influence of soil water, clay, temperature, and carbonate minerals on soil electrical conductivity readings with an EM-38 along a Mollisol catena in central Iowa. Soil. Surv. Hori. 43, 9–13.

Brogi, C., Huisman, J.A., Pätzold, S., von Hebel, C., Weihermüller, L., Kaufmann, M.S., van der Kruk, J., Vereecken, H., Large-scale soil mapping using multi-configuration EMI and supervised image classification, Geoderma, Volume 335, 2019, Pages 133-148, ISSN 0016-7061, https://doi.org/10.1016/j.geoderma.2018.08.001

Calinski, T. and Harabasz, J. A dendrite method for cluster analysis. Communications in Statistics, 3, 1–27, 1974.

Chang, C-W, Laird, DA, Mausbach, MJ, Hurburgh, CR. Near-infrared reflectance spectroscopy principal components regression analyses of soil properties. Soil Sci Soc Am J. 2001;65:480-90. https://doi.org/10.2136/sssaj2001.652480x

Doolittle, J. A., Brevik, E. C. The use of electromagnetic induction techniques in soils studies, Geoderma, Volumes 223–225, 2014, Pages 33-45, ISSN 0016-7061, https://doi.org/10.1016/j.geoderma.2014.01.027.

Rodrigues, F.A., Bramley, R.G.V., Gobbett, D.L., Proximal soil sensing for Precision Agriculture: Simultaneous use of electromagnetic induction and gamma radiometrics in contrasting soils, Geoderma, Volumes 243–244, 2015, Pages 183-195, ISSN 0016-7061, https://doi.org/10.1016/j.geoderma.2015.01.004

Terra, F.S., Demattê, J.A.M., Viscarra Rossel, R.A. Spectral libraries for quantitative analyses of tropical Brazilian soils: comparing vis–NIR and mid-IR reflectance data. Geoderma, Amsterdam, 255–256 (2015), pp. 81-93, 10.1016/j.geoderma.2015.04.017.

Franke, R. 1982. Smooth Interpolation of Scattered Data by Local Thin Plate Splines. Computer and Mathematics with Applications. Vol. 8. No. 4. pp. 273–281. Great Britain.

Heil, K., Schmidhalter, U., 2012. Characterisation of soil texture variability using the apparent soil electrical conductivity at a highly variable site. Comput. Geosci. 39, 98–110.

Guagliardi, I., Rovella, N., Apollaro, C., Bloise, A., De Rosa, R., Scarciglia, F., Buttafuoco, G., Effects of source rocks, soil features and climate on natural gamma radioactivity in the Crati valley (Calabria, Southern Italy), Chemosphere, Volume 150, 2016, Pages 97-108, ISSN 0045-6535, https://doi.org/10.1016/j.chemosphere.2016.02.011

Mendes, W. de S., Medeiros Neto, L. G., Demattê, J.A.M., Gallo, B. C., Rizzo, R., Safanelli, J. L., Fongaro, C. T., Is it possible to map subsurface soil attributes by satellite spectral transfer models? Geoderma, Volume 343, 2019, Pages 269-279, ISSN 0016-7061, https://doi.org/10.1016/j.geoderma.2019.01.025

Mezzalira, S. (1989). Os fósseis do Estado de São Paulo. São Paulo, Secretaria do Meio Ambiente/Instituto Geológico. 2.ed. Série Pesquisa. 142p.

Karchegani, P. M., Ayoubi, S., Lu, S. G., Honarju, N., Use of magnetic measures to assess soil redistribution following deforestation in hilly region, Journal of Applied Geophysics 75 (2011) 227–236, doi:10.1016/j.jappgeo.2011.07.017

Quinlan. Learning with continuous classes. Proceedings of the 5th Australian Joint Conference On Artificial Intelligence (1992) pp. 343-348.

Romero-Ruiz, A., Linde, N., Keller, T., Or, D., 2018. A review of geophysical methods for soil structure characterization. Rev. Geophys. 56, 1–26.

Salazar, D. F. U., Demattê, J.A.M., Vicente, L. E., Guimarães, C. C.B., Sayão, V. M., Cerri, C.E.P., Padilha, M. C. de C., Mendes, W. De S., Emissivity of agricultural soil attributes in southeastern Brazil via terrestrial and satellite sensors, Geoderma, Volume 361, 2020, 114038, ISSN 0016-7061, https://doi.org/10.1016/j.geoderma.2019.114038

Sayão, V. M., Demattê, J.A.M., Bedin, L. G., Nanni, M. R., Rizzo, R. Satellite land surface temperature and reflectance related with soil attributes, Geoderma, Volume 325, 2018, Pages 125-140, ISSN 0016-7061, https://doi.org/10.1016/j.geoderma.2018.03.026.

Stadler, A., Rudolph, S., Kupisch, M., Langensiepen, M., van der Kruk, J., Ewert, F., Quantifying the effects of soil variability on crop growth using apparent soil electrical conductivity measurements, European Journal of Agronomy, Volume 64, 2015, Pages 8-20, ISSN 1161-0301, https://doi.org/10.1016/j.eja.2014.12.004.

Sudduth, K.A., Kitchen, N.R., Myers, D.B., Drummond, S.T., 2010. Mapping depth to argillic soil horizons using apparent electrical conductivity. J. Environ. Eng. Geophys. 15 (3), 135–146.

Tajik, S., Ayoubi, S., Zeraatpisheh, M., Digital mapping of soil organic carbon using ensemble learning model in Mollisols of Hyrcanian forests, northern Iran, Geoderma Regional, 2020, e00256, ISSN 2352-0094, https://doi.org/10.1016/j.geodrs.2020.e00256.

Yang, H., Zhang, X., Xu, M, Shao, S., Wang. X., Liu, W., Wu, D., Ma, Y., Bao, Y., Zhang, X., Liu, H. Hyper-temporal remote sensing data in bare soil period and terrain attributes for digital soil mapping in the Black soil regions of China, CATENA, Volume 184, 2020, 104259, ISSN 0341-8162, https://doi.org/10.1016/j.catena.2019.104259.